698978

B. G. Schappell

ADC and Reviewing Official
B. G. Schappell, Mgr. GEE

9/19/94

EPD-SGS-94-307
Rev. 0

URANIUM GEOCHEMISTRY IN SOIL AND GROUNDWATER AT THE F AND H SEEPAGE BASINS (U)

UNCLASSIFIED

Does Not Contain Unclassified Controlled Nuclear Information (UCNI)

September 1994

Westinghouse Savannah River Company
Savannah River Site
Aiken, SC 29808

Prepared for the U. S. Department of Energy under Contract No. DE-AC09-89SR18035

SAVANNAH RIVER SITE · SAFETY · RESPONSIBILITY · SECURITY

EPD-SGS-94-307
Rev. 0

URANIUM GEOCHEMISTRY IN SOIL AND GROUNDWATER AT THE F AND H SEEPAGE BASINS (U)

Revision 0 Prepared by:

Steven M. Serkiz — 9/19/94 Date

William H. Johnson — 9/19/94 Date

Reviewed and Approved by:

Bruce G. Schappell — 9/19/94 Date

Bruce G. Schappell
Manager, Geo-Environmental Engineering

Westinghouse Savannah River Company
Savannah River Site
Aiken, SC 29808

Prepared for the U. S. Department of Energy under Contract No. DE-AC09-89SR18035

SAVANNAH RIVER SITE · SAFETY · RESPONSIBILITY · SECURITY

DISCLAIMER

Westinghouse Savannah River Company
Savannah River Site
Aiken, SC 29808

Prepared for the U. S. Department of Energy under Contract No. DE-AC09-89SR18035

EXECUTIVE SUMMARY

For 33 years, low activity liquid wastes from the chemical separation areas at the U. S. Department of Energy's Savannah River Site were disposed of in unlined seepage basins. Soil and associated pore water samples of widely varying groundwater chemistries and contaminant concentrations were collected from the region downgradient of these basins using cone penetrometer technology. Analysis of samples using inductively coupled plasma - mass spectrometry has allowed the investigation of uranium partitioning between the aqueous phase and soil surfaces at this site. The distribution of uranium was examined with respect to the solution and soil chemistry (e.g., pH, redox potential, cation and contaminant concentration) and aqueous-phase chemical speciation modeling.

The uranium soil source term at the F- and H-Area Seepage Basins (FHSB) is much smaller than has been used in pervious modeling efforts. All other geochemical conditions being equal, this should result in a much shorter remediation time and a greater effectiveness of a pump-and-treat design than previously predicted.

Distribution coefficients at the (FHSB) were found to vary between 1.2 to 34,000 l kg^{-1} for uranium. Differences in sorption of these elements can be explained primarily by changes in aqueous pH and the associated change in soil surface charge. The inflection point of the sorption isotherm occurs at about pH = 4.0. This means that at a pH below 4, most of the uranium in solution, while above a pH of 4, most of the uranium is bound to the soil surface.

Sorption models were fit directly to sorption isotherms from field samples. All models underestimated the fraction of uranium bound at low aqueous uranium concentrations. Linear models (e.g. single K_d, Langmuir) overestimated bound uranium at locations where the aqueous concentration was greater than 500 ppb. Mechanistic models(e.g. diffuse-layer, variable charge constant capacitance) provided a much better estimate of the bound uranium concentrations, especially at high aqueous concentrations. The observed field data was found to be best fit by a simple empirical model which varies with pH. Models fit to the field derived data showed an improvement of over two orders of magnitude, as measured by the sum of errors squared, when compared with the single $K_d = 40$ model used in previously.

Since a large fraction of the uranium at the site is associated with the low-pH portion of the plume, substantial portions of the total uranium mass could be more easily removed before the pH of the system returns to more natural conditions. Therefore, consideration should be given to pumping water from the lowest pH portions of the plume in the F-Area. Finally, because uranium mobility is highly dependent on aqueous pH and carbonate concentration, a strategy that useds the chemistry of the reinjection water to either mobilize or immobilize contaminants should be developed.

Keywords: sorption, speciation, geochemistry, uranium, F and H Seepage Basins

CONTENTS

LIST OF FIGURES

LIST OF TABLES

1.0 INTRODUCTION

To properly assess the risk associated with a waste site and to accurately assess potential remedial alternatives, knowledge of the geochemical transport characteristics of each contaminant is required. Even contaminants that are initially soluble in water may not travel through the subsurface environment at the same velocity as the water due to the processes of solid-phase sorption and precipitation. Therefore, to accurately predict contaminant transport a knowledge of both aqueous- and solid-phase speciation is necessary.

This study has been designed to generate site-specific transport factors for contaminated groundwater downgradient of the F and H Area Seepage Basins (FHSB). This report describes the results of this study for uranium. In particular, this report addresses the following subjects:

- quantification of the amount of uranium bound to soil surfaces (i.e., the soil source term);
- a description of the aqueous-phase speciation of uranium in groundwater at the basins; and
- an investigation of the geochemistry controlling the partitioning of uranium between the groundwater and soil surfaces at the basins.

The experimental approach of this study was to collect soil and its associated porewater from contaminated areas downgradient of the FHSB. Samples were collected over a wide range of geochemical conditions (e.g., pH, conductivity, and contaminant concentration) and were used to describe the partitioning of contaminants between the aqueous phase and soil surfaces at the site. The partitioning behavior was then used to develop defensible site-specific transport factors.

The site-specific transport factors derived from this study can be used to update the current flow and transport models in order to better evaluate remedial alternatives and calculate risk levels at this site.

This report is organized as follows:

- Section 1 is the introduction including the waste site background, risk drivers, and a conceptual hydrogeochemical model of the site;
- Section 2 describes the experimental approach taken to collect data on the geochemistry of the FHSB;

- a mathematical description of the models employed for both aqueous-phase and surface-sorption processes is presented in Section 3;
- the results of field and laboratory analytical data and the calculations and modeling used to evaluate the geochemistry at the FHSB are contained in Section 4;
- Section 5 contains a summary of data and conclusions; and
- descriptions of on going work and recommendations from this study are presented in Section 6.

1.1 Waste Site Background

From 1955 until 1988, the FHSB received process waste water and storm-water runoff from the tritium and plutonium separation facilities at the Savannah River Site in South Carolina. The unlined basins were designed to allow the natural processes of evaporation and infiltration to dispose of the polluted effluent streams. This has resulted in groundwater in the vicinity of these basins exhibiting lowered pH values and elevated concentrations of metals, radionuclides, nitrate, and sodium as compared to background water quality.

On November 7, 1988, discharge to the basins was terminated in accordance with requirements of Resource Conservation and Recovery Act. Before a multi-layered cap was placed over the basins, the liquid was removed and each basin was filled with a gravel bed topped with layers of calcium carbonate and blast furnace slag. The carbonaceous rock was intended to raise the pH of the naturally infiltrating rainwater to a pH of between 8 and 9, while the slag, a source of reduced iron and sulfides, should lower the redox potential of the water. Under these conditions of high pH and low Eh, heavy metals were expected to precipitate from solution (Closure Plan for the F-Area Hazardous Waste Management Facility, WSRC, Aiken, SC).

1.2 Constituents of Concern and Risk Drivers

The constituents of concern for the FHSB as determined in the baseline CERCLA risk assessment are presented in Table 1-1, along with the partitioning coefficients used in groundwater modeling for the waste unit (GeoTrans 1991a).

Risk associated with the FHSB was evaluated in the Remedial Alternative Risk Assessment for the F- and H-Area Seepage Basins Groundwater Unit (WSRC 1992a). The results of this analysis are summarized in Tables 1-2 to 1-5. All risk levels were taken from the ingestion of groundwater by a hypothetical on-site resident and the long-term drivers were evaluated at the 100 and 1000 year time step.

Table 1-1. Distribution coefficient values (Kd) currently used in groundwater modeling of F- and H-Area contaminants of concern. Adapted from Looney (1985).

Contaminant	Typical value for SRS	Range of reported values
Inorganics		
Aluminum	5[1]	Not reported
Arsenic	3	1 - 10
Barium	5[1]	530, 2800
Cadmium	6	1 - 900
Chromium	40	1 - 1000
Copper	25	1 - 100
Fluoride	0.001	Not reported
Iron	5[1]	Not reported
Lead	100	1 - 10,000
Manganese	5[1]	Not reported
Mercury	15[1]	10,000 - 1,000,000
Nickel	100	10 - 1000
Nitrate	0.001[1]	Not reported
Selenium	2.5	1 - 100
Silver	100	10 - 100
Zinc	16	0.1 - 10,000
Organics		
Cyanide	0.01	Not reported
Phenol	0.003[1]	Not reported
C_2Cl_4	0.022	Not reported
Radionuclides		
Cs-137	500	10 - 100,000
Cm-243	3000	100 - 100,000
H-3	0.001	0.000001 - 0.001
I-129	0.2	0.001 - 1
Ra-226	100	10 - 1,000,000
Ra-228	100	10 - 1,000,000
Sr-90	8	1 -1000
Th-228	100	10 - 100,000
U-234	40	0.1 - 1,000,000
U-238	40	0.1 - 1,000,000

[1]"Best guess" value per personnel communication between GeoTrans, Inc. and David Nix.

Table 1-2 F-Area Carcinogenic Risk

	Present		100 Year		1000 Year	
Constituent	Risk	% Tot	Risk	% Tot	Risk	% Tot
Uranium-238	5E-3	66	4E-3	80	1E-3	80
Uranium-234	7E-4	10	6E-4	10	3E-5	10
Radium-228	2E-4	4	2E-4	8	3E-5	10

Source: Remedial Alternative Risk Assessment for the F- and H-Area Seepage Basins Groundwater Unit (WSRC 1992a).

Table 1-3 F-Area Noncarcinogenic Risk

	Present		100 Year		1000 Year	
Constituent	Haz Ind	% Tot	Haz Ind	% Tot	Haz Ind	% Tot
Lead	1000	99	1100	99	1100	99
Manganese	80	LT 1	30	LT 1	10	LT 1
Copper	20	LT 1	20	LT 1	10	LT 1
Mercury	10	LT 1	10	LT 1	10	LT 1

Source: Remedial Alternative Risk Assessment for the F- and H-Area Seepage Basins Groundwater Unit (WSRC 1992a).

Table 1-4 H-Area Carcinogenic Risk						
	Present		100 Year		1000 Year	
Constituent	Risk	% Tot	Risk	% Tot	Risk	% Tot
Strontium-90	5E-4	40	2E-5	2	1E-7	0
Radium-226	5E-4	40	5E-4	50	5E-4	99
Iodine-129	1E-4	10	9E-5	10	LT E-8	0
Tritium	9E-5	10	LT E-8	0	LT E-8	0

Source: Remedial Alternative Risk Assessment for the F- and H-Area Seepage Basins Groundwater Unit (WSRC 1992a).

Table 1-5 H-Area Noncarcinogenic Risk						
	Present		100 Year		1000 Year	
Constituent	Haz Ind	% Tot	Haz Ind	% Tot	Haz Ind	% Tot
Lead	1000	99	5000	96	5000	96
Copper	5	LT 1	100	2	90	2
Mercury	100	1	90	2	90	2

Source: Remedial Alternative Risk Assessment for the F- and H-Area Seepage Basins Groundwater Unit (WSRC 1992a).

For the F-Area Seepage Basins the predicted carcinogenic risk level over the 1000-year period is clearly dominated by uranium contamination. At the H-Area Seepage Basins, where aqueous uranium concentrations are much lower, the carcinogenic risk is spread out among a number of radionuclides. The non-carcinogenic risk in both areas is predicted to be dominated by lead.

The presence of high uranium concentrations at the F-Area Seepage basins and its high projected risk level were major considerations in evaluating its geochemistry in greater detail.

1.3 CONCEPTUAL HYDROGEOCHEMICAL MODEL

Attempts to select an appropriate remediation technology for groundwater at this site have been hampered by an inability to adequately predict the transport of pollutants through, and the amount of contaminants in, the subsurface environment. The models currently being utilized for risk assessment use single literature reported or "best guess" K_d values. Because little data existed for the concentrations and distribution of contaminants in the solid phase (i.e., in the soils) for the FHSB, "best guess" K_d values were used to calculate the soil concentration of contaminants based on observed groundwater concentrations (GeoTrans 1991b). Therefore, these models predicted very large source terms for constituents with high K_d values and that these contaminants should be sorbed by the soil and not substantially transported (GeoTrans 1991b). In actuality, soil cores collected from directly beneath the basins (Corbo, et. al., 1985) contained much lower concentrations of many contaminants than was predicted by the models and significant groundwater transport of some contaminants (e.g. cesium, lead, mercury) from the site has been observed (WSRC 1992b; WSRC 1992c), although little transport was predicted.

This apparent failure of model predictions using literature K_d values stems largely from the fact that the geochemical conditions downgradient of the basins are much different (low pH and high ionic strength) than the conditions under which the literature K_d values were determined and the operations of the basins has significantly altered the soil surfaces by stripping and/or precipitating surface mineral coatings.

The waste discharged to the FHSB was generally acidic with a high salt concentration. Typically, waste solution pH values were approximately 2.6 with NO_3^- and Na^+ concentrations of 880 ppm and 400 ppm respectively (Ryan 1984). Under these conditions, the soil coatings and matrix are expected to be highly altered. This is especially true of the very fine, high surface area clay fraction. X-ray diffraction analysis of the < 2 μm fraction of several samples collected in this study show that clay fraction of soil in the vicinity of FHSB is primarily kaolinite [$Si_4Al_4O_{10}(OH)_8$] (Johnson, 1994). The iron oxides hematite [Fe_2O_3] and goethite [FeOOH] are present as surface coatings on these soils leading to the typical reddish brown coloration. Dissolution of the soil coating and matrix is evident from changes in the groundwater chemistry as it flows away from the basins. Downgradient of the basins, the pH of the system is slightly higher as the

concentration of H^+ ions in the acidic waste water has been replaced by Al^{3+}, Si^{4+}, Fe^{3+}, Na^+ ions from the soil matrix.

As groundwater concentrations of common soil matrix ions and the pH values increase, precipitation of new minerals is expected to occur. Based on thermodynamic speciation modeling (discussed in greater detail below), groundwater downgradient of the FHSB is currently oversaturated with respect to several types of Si, Fe, and Al based minerals and oxides. The precipitation of these mineral phases is expected to occur on existing soil surfaces, resulting in the formation of new reactive surfaces. These new coatings will influence future binding of contaminants in the plume.

2.0 EXPERIMENTAL APPROACH

The basic experimental approach in this study was to collect soil and its associated porewater from contaminated areas downgradient of the FHSB. Samples were collected over a wide range of geochemical conditions (e.g., pH, conductivity, and contaminant concentration) and were used to describe the partitioning of contaminants between the aqueous phase and soil surfaces at the site. The intent was that the partitioning behavior of each contaminant could be used to develop defensible site-specific transport factors.

2.1 Sampling

A total of 56 sets of soil and porewater samples and 32 vadose zone samples were collected for this study. Samples were collected using an electric friction-cone penetrometer system with a hydrocone (Edge and Cordy 1989) or geocone depending on media to be sampled. All hydrocone porewater samples were collected under a constant backpressure applied with argon. The argon gas ensured inert conditions were maintained until the sample was drawn to the surface. Samples sets (i.e., soil and its associated porewater) from the saturated zone downgradient of the waste sites were collected from the same depth, at the same location. Replicate samples (i.e. saturated zone sample pairs and soil samples from the vadose zone) were collected at ten percent of the sampling locations selected on a random basis.

Sampling locations and depths were selected such that they spanned a range of groundwater pH (pH=3-7) and major ion chemistries, and had previously exhibited groundwater contaminant concentrations above the analytical detection limits. The areal view of the sampling transects, along with pH and RCRA metals isoconcentration contours are shown in Figures 2-1 and 2-2 for the F and the H Areas respectively. The cross sections for each of these sampling transects are shown in Figures 2-3 through 2-8 for transects A through F, respectively.

All samples collected in the field were identified by a 4 digit sample identification number. The first letter in a sample name (A-F) represents the transect from which it came. The second number (1-5) is the hole in the transect, whereas the third number (1-4) is the relative sampling depth from which the sample came. The forth digit represents the type of sample; 'S' for soil, 'W' for water. For instance, sample C42W is a water sample from the second depth (48 feet) at CPT location C4. Table 2-1 lists site coordinates of CPT sampling locations and depths of all samples.

Two uncontaminanted background soil samples representative of the same lithographic unit sampled downgradient of the FHSB were collected from the Little Grand Canyon area which is upgradient of F-Area. The soils were collected from an outcropping at a height of approximately 20 feet above the tan clay layer. This depth is equivalent to that of the deeper samples in this work. These samples were given the designation GC4 and GC5 after a sample labeling scheme already in use in another study at the collection site. Both samples were characterized in terms of their physical and chemical properties.

2.2 Analysis

Immediately upon obtaining water samples, temperature, pH, redox potential, and conductivity of the sample were measured. Temperature and pH were measured using a pH meter with a built in temperature monitor. Redox potential was measured directly using a combination platinum electrode. Porewater samples were stored in acid-washed 1-l LDPE bottles. Soil samples were double bagged into 4-l zip-lock bags. Both porewater and soil samples were then stored in a cooler on ice until the end of the day. After Health Protection personnel verified that the beta and gamma count rates were not above background levels, the samples were transported to a dark sample storage cooler which was temperature regulated at 4°C.

Within a week of sampling, two 10-ml aliquots of each porewater sample were filtered using 0.45 μm syringe filters. Both of these aliquots were analyzed for ^{3}H using liquid scintillation counting, and Cl^-, F^-, NO_3^-, PO_4^{3-}, and SO_4^{2-} concentrations using ion chromatography. A 60-ml aliquot of the sample was analyzed for organic and inorganic carbon using an automated carbon analyzer.

The remaining sample was filtered through a 0.45 μm cellulose nitrate membrane and acidified to 1% v/v with 70% ultra-pure HNO_3. The acidified samples were analyzed quantitatively using inductively coupled plasma (argon) mass spectrometry (ICP-MS) for 43 isotopes representing 28 elements. Additionally, a semi-quantitative ICP-MS scan for the isotopes of Hg and the actinides (mass less than 246) was also performed. 500 ml of the acidifed sample was placed in a 1-l Marinelli beaker to enable the sample to be analyzed by gamma spectrophotometry.

Physical and chemical properties of the soil samples examined included total elemental analysis, soil pH, particle size distribution, carbon content, cation exchange capacity, and hygroscopic moisture content. Additionally, gamma spectrophotometry was performed on a 200 cm^3 aliquot of most samples.

Each soil sample was prepared for total elemental analysis using the hydrofluoric acid digestion procedure outlined by Lim (1982). Samples were prepared in triplicate by digesting approximately 200 mg of soil in 1 ml of ultra-pure aqua regia and 10 ml of ultra-pure HF. Samples were then heated at 100°C for 3 hours, filtered through 0.45 μm Teflon filters, and diluted to 50 ml with deionized water. After ICP-MS analysis, as outlined above, contaminant concentrations in the total digestion extract were converted to soil concentrations by multiplying by a conversion factor equal to the extract volume divided by the digested sample weight.

Particle size analysis of each soil sample was performed using the method presented by Gee (1986). Two 40-g aliquots of each sample were prepared for analysis by removing surface coatings and cementing agents. Dispersion of the soil particles was facilitated by shaking the soil overnight in a sodium phosphate solution. The distribution of the sand

fraction (>53 μm) of each sample was determined by passing the dispersed sample through a series of brass sieves. All rinsings which passed through the smallest (53μm) sieve were analyzed to determine amount and distribution of the clay (<2 μm) and silt (2 - 53 μm) fractions using a pipet-sedimentation method. Data from the two replicates was averaged to obtain the sand, clay and silt fractions.

The cation exchange capacity of each soil sample was measured in duplicate using the barium-magnesium exchange technique described by Rhoades (1982). A 2-g portion of soil was saturated with barium by equilibration with a $BaCl_2$ solution at a pH of 4.5. The soil was then reacted with $MgSO_4$ which replaced the sorbed Ba with Mg. The amount of Mg sorbed per unit weight of soil is equivalent to the cation exchange capacity and is reported in meq kg^{-1}.

Soil pH was determined in using ASTM procedure D4972-89 (ASTM, 1989).

ICP-MS allows the determination of elemental concentrations of up to 70 elements at ng l^{-1} concentrations with minimal sample volume. The analysis method uses a plasma torch to ionize the sample by heating it to 8000°K. The cations are drawn through a low vacuum interface into a mass spectrometer which determines the isotopic concentration by the charge to mass ratio of the cations. Elemental concentrations can then be calculated by correcting for the natural abundance of an isotope and the ability of an element to be ionized. Interferences occur at atomic mass numbers where two or more elements have isotopes or masses where doubly ionized atoms are present. Prior to analysis, each sample, standard, or blank, was spiked with a series of elements at known concentrations. Based on counts obtained from these internal standards, calculated concentrations are normalized to account for instrument response changes.

Because the instrument is designed to detect individual atoms rather than solution activity or number of atoms decaying, the detection limit of ICP-MS is outstanding for metals and long-lived radionuclides. Many elements may be analyzed for by monitoring more than one isotope. The detection limit for a given element was determined daily. It is influenced by the alignment and sensitivity of the instrument, the background counts and natural isotopic abundance of the isotope being examined, and ionization potential of the element. In this study, instrument response to uranium concentration was linear over the entire quantification range. Typically, the minimum standard concentration used was 50 ng l^{-1}. This is equivalent to 0.6 mBq l^{-1} of ^{238}U or 4 mBq l^{-1} of ^{235}U. The minimum detectable level was assumed to be equal to the lower quantification limit.

Concentrations of ^{235}U and ^{238}U are reported separately. Distribution coefficients for each sample were calculated by dividing the soil concentration of an isotope (in μg kg^{-1}) by the concentration of that element or isotope in the associated porewater sample (in μg l^{-1}). No distinction was made between anthropogenic and naturally occurring uranium. This could result in an over-estimation of reported in-situ K_d values as uranium concentrations associated with the soil matrix are included in the reported soil concentration.

2.3 Idealized Surface Sorption Studies

As stated previously, the operation of the basins is expected to have significantly altered soil sorption sites on the surfaces of soils at the basins.

Based on thermodynamic modeling, aluminum oxyhydroxide minerals are expected to be the first precipitates from the FHSB groundwater. The first crystalline mineral is expected to be gibbsite [$Al(OH)_3$]. Boehmite [AlOOH] and diaspore, an isomer of boehmite, are also expected. This is consistent with other locations where soils have been highly weathered by natural processes (Bear 1964).

Because stability constants for uranium sorption to gibbsite could not be found in the literature, a laboratory study was initiated to generate these constants for further modeling efforts. In this study, fresh gibbsite was prepared by precipitation from an $Al(NO_3)_3$ solution by adjusting the pH with 50 percent w/w sodium hydroxide (Anderson and Benjamin, 1990). The gibbsite was purified by dialysis to remove the excess sodium nitrate salts and lyophilized for storage as a dry powder. The gibbsite was characterized using x-ray diffraction and thermogravimetric analyses. Uranium sorption to this material was conducted using a batch approach in a carbonate free environment. The gibbsite to solution ratio was 1 g l^{-1}. Factors affecting uranium sorption that were investigated included: (1) aqueous uranium concentration; (2) pH; and (3) backing electrolyte concentration (i.e., ionic strength effects).

The initial results of this study have been incorporated into this report and will be discussed in a later section.

Table 2-1. Cone penetrometer test sampling locations and depths.

CPT label	East Site Coordinate	North Site Coordinate	Ground Elevation (feet)	depth to water table (feet)	first vadose zone Soil Sample (feet)	second vadose zone Soil Sample (feet)	depth to first Water Sample (feet)	depth to first saturated Soil Sample (feet)	depth to second Water Sample (feet)	depth to second saturated Soil Sample (feet)
*A1	50095	75396	281	68	63	NA	73	75	88	90
A2	50041	74990	282	71	66	NA	76	78	91	93
A3	49997	74633	261	51	NA	NA	56	58	71	73
A4	50005	74227	241	34	NA	NA	39	41	54	56
A5	49899	73896	215	24	18	NA	28	30	38	40
B1	51100	75372	277	63	48	58	68	70	78	80
B2	51088	75269	276	62	47	57	67	69	77	79
B3	51072	75125	269	56	51	NA	61	63	71	73
B4	51049	74919	259	48	43	NA	53	55	73	75
B5	51016	74623	245	35	NA	NA	40	42	55	57
C1	51374	75563	279	62	24	57	67	69	82	84
C2	51403	75443	277	60	55	NA	65	67	80	82
C3	51433	75319	267	51	46	NA	56	58	71	73
C4	51492	75075	258	43	38	NA	48	50	63	65
D1	50215	75568	282	68	32	63	102	104	NA	NA
D2	50158	75486	282	68	63	NA	NA	NA	NA	NA
*D3	50095	75396	281	68	63	NA	NA	NA	NA	NA
D4	49952	75191	284	72	67	NA	NA	NA	NA	NA
D5	49786	74953	280	69	64	NA	NA	NA	NA	NA
E1	57029	71706	262	39	29	34	44	46	49	51
E2	56965	71612	259	37	27	32	42	44	47	49
E3	56880	71487	243	23	13	18	28	30	33	35
E4	56795	71242	222	4	NA	NA	9	11	14	16
F1	58688	72057	259	28	23	NA	30	32	35	37
F2	58621	71982	257	27	22	NA	29	31	34	36
F3	58480	71874	254	25	20	NA	27	29	32	34
F4	58223	71535	247	22	17	NA	27	29	32	34
F5	57862	71227	238	18	13	NA	21	23	26	28

* Intersection of transects 'A' and 'D'.

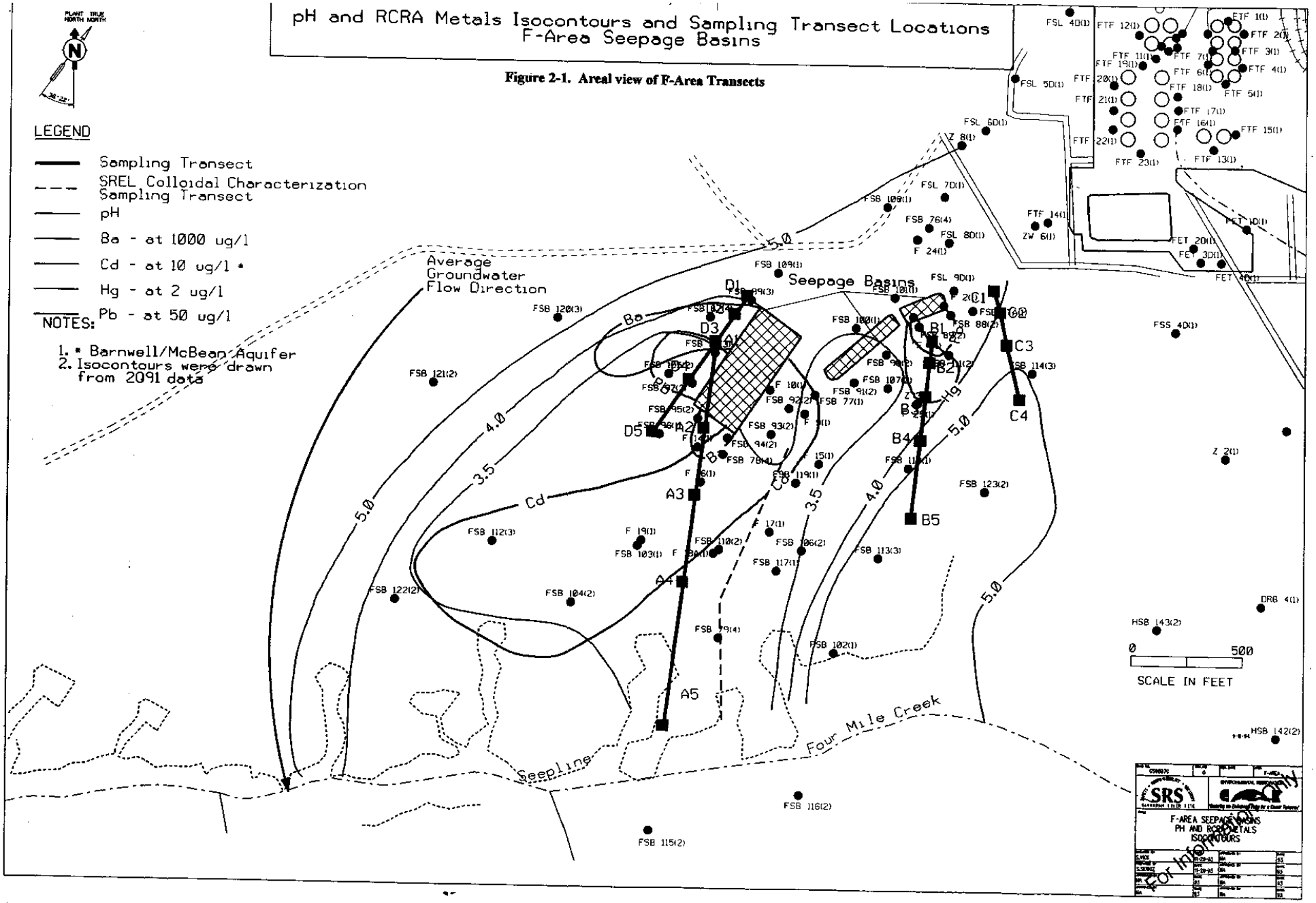

Figure 2-1. Areal view of F-Area Transects

pH and RCRA Metals Isocontours and Sampling Transect Locations H-Area Seepage Basins

Figure 2-2. Areal view of H-Area Transects

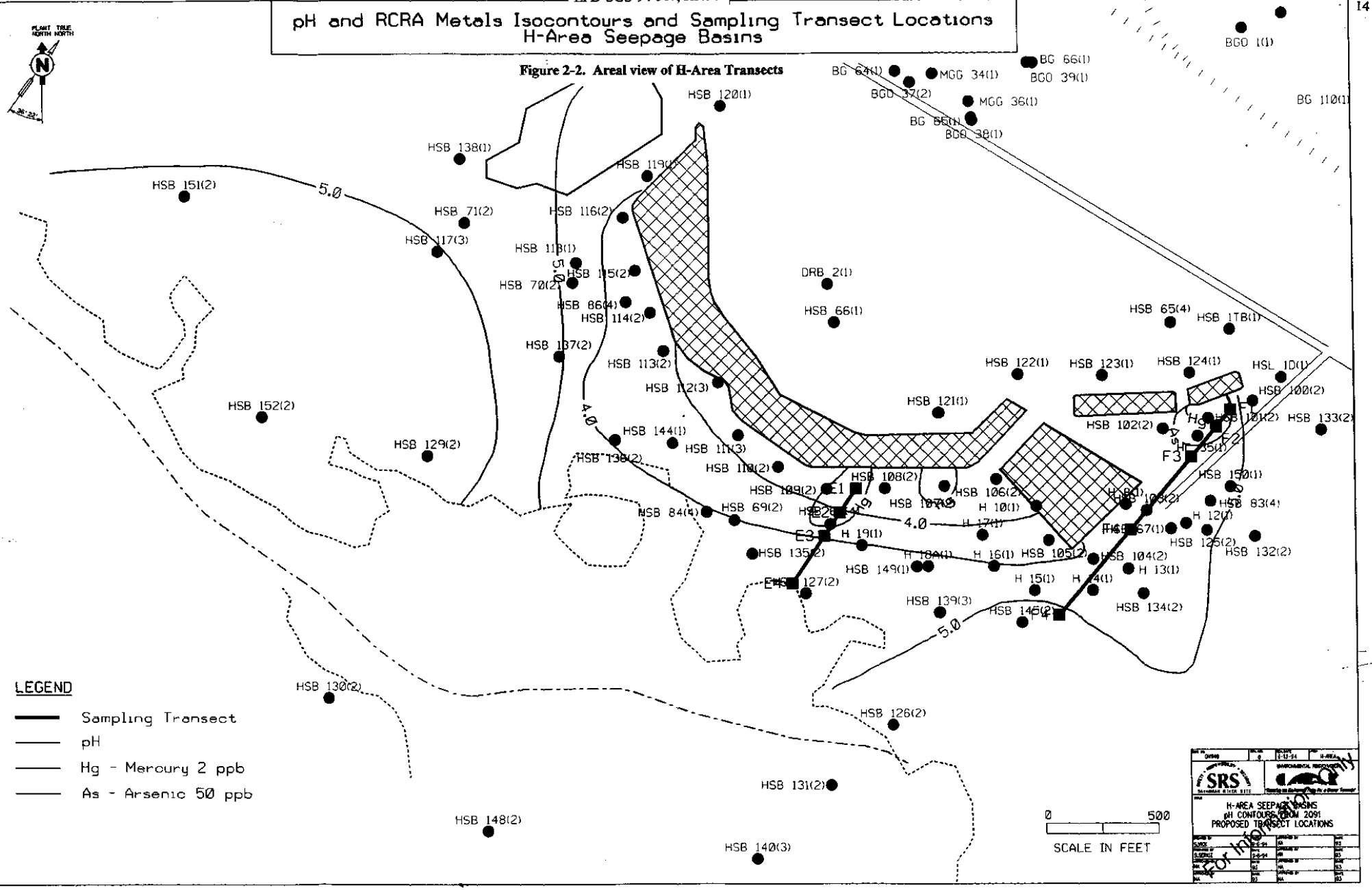

Figure 2-3 Cross section of Transect A-A'

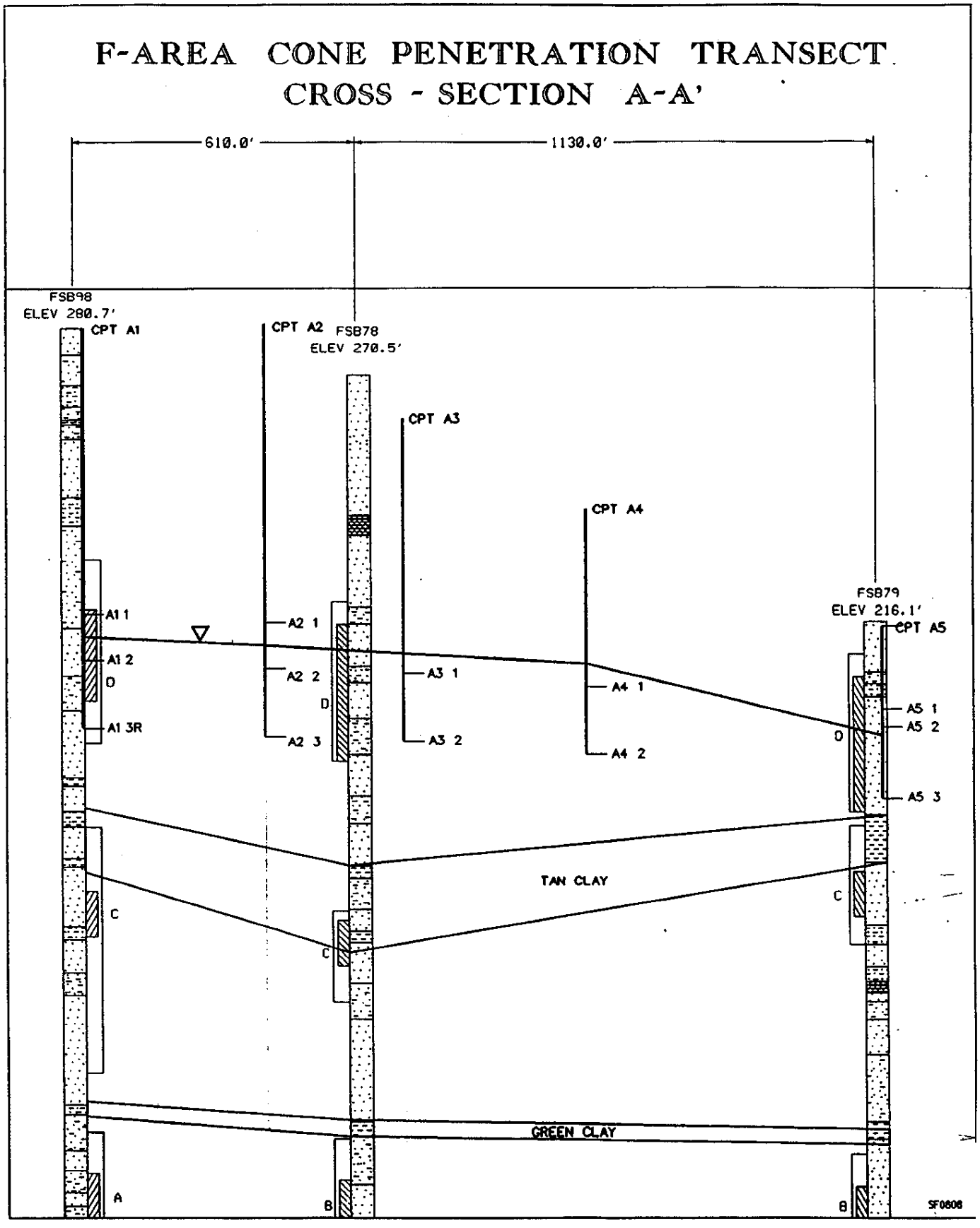

Figure 2-4 Cross section of Transect B-B'

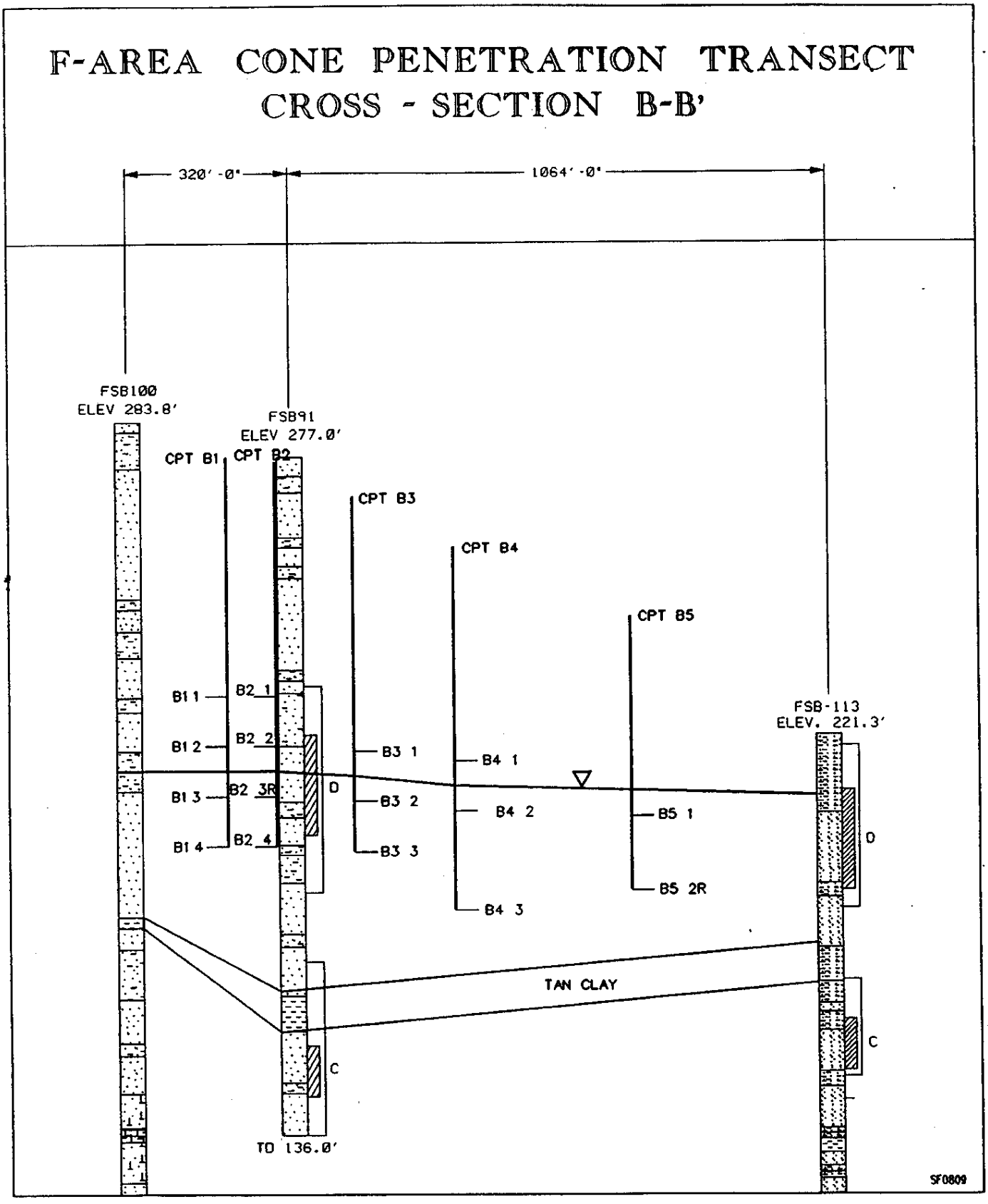

Figure 2-5 Cross section of Transect C-C'

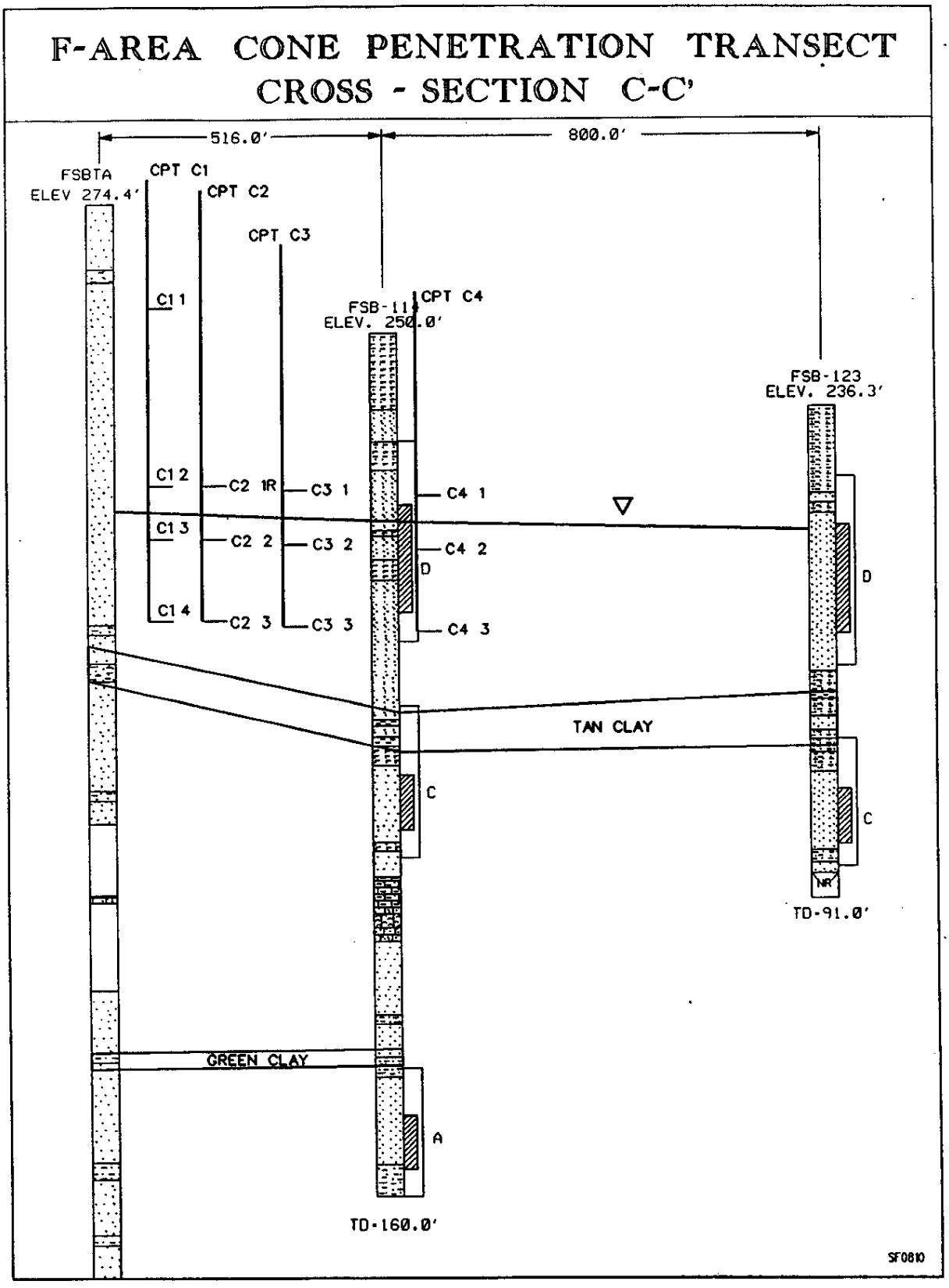

Figure 2-6 Cross section of Transect D-D'

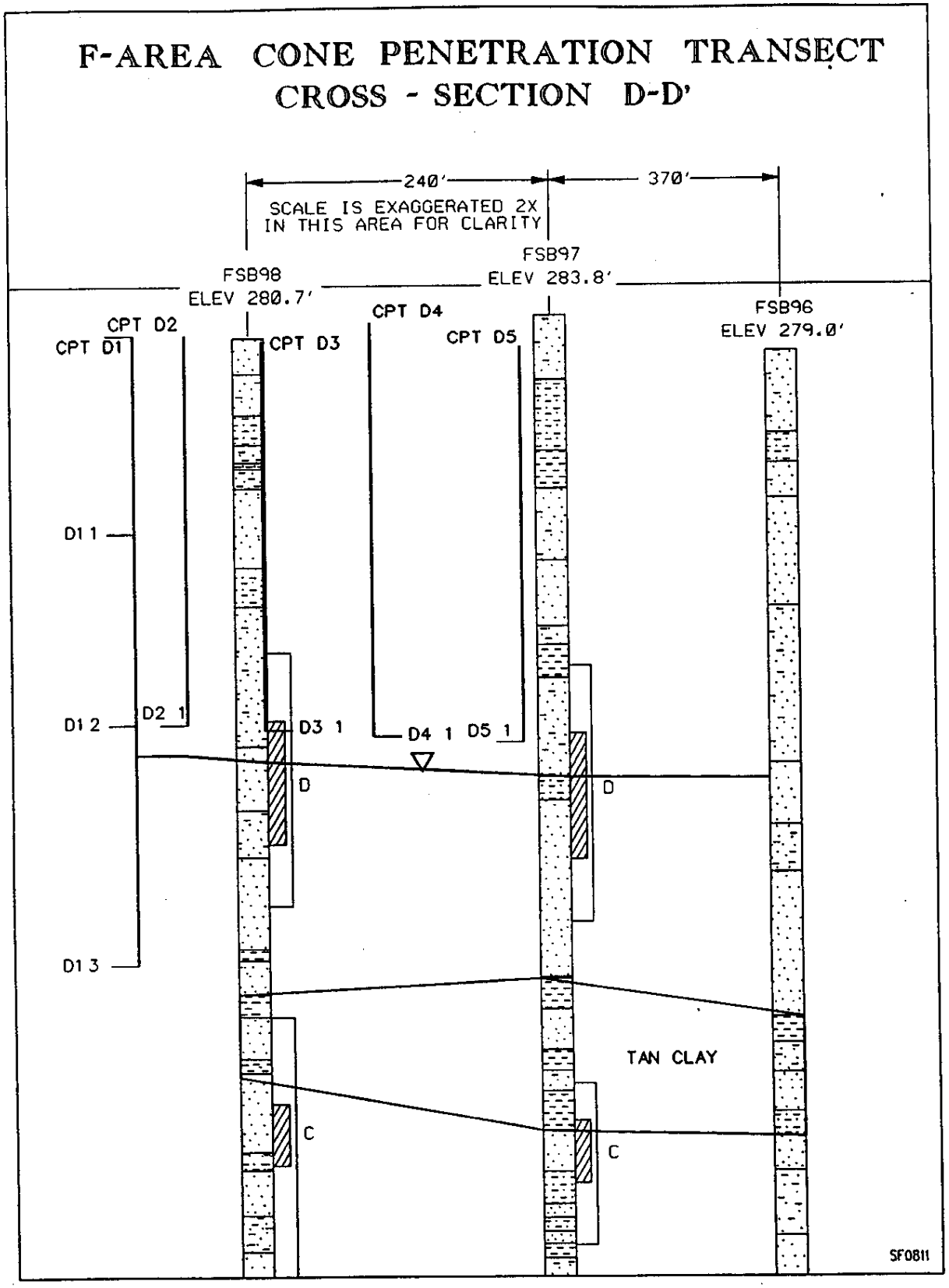

Figure 2-7 Cross section of Transect E-E'

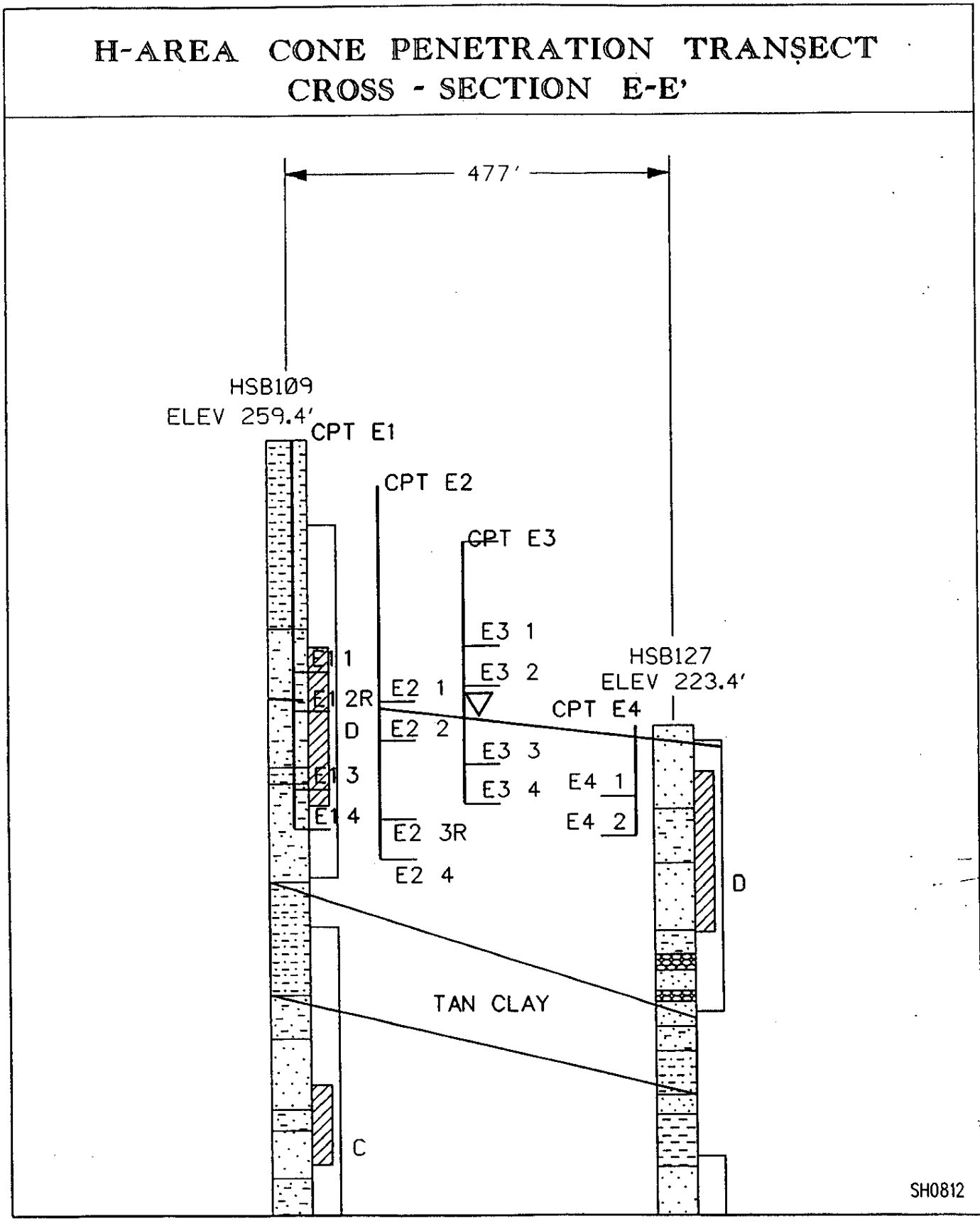

Figure 2-8 Cross section of Transect F-F'

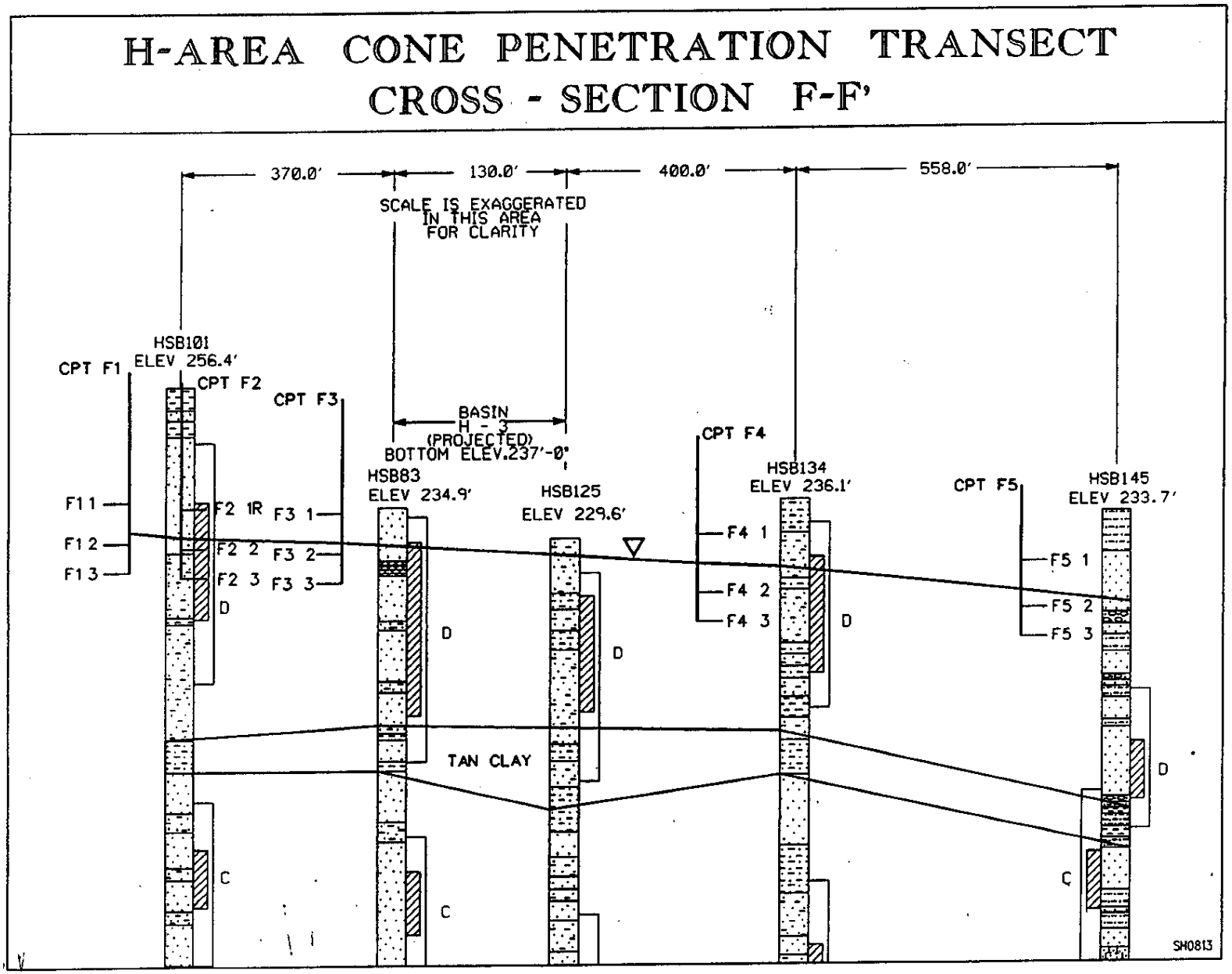

3.0 SPECIATION MODELING BACKGROUND

The chemical form in which a molecule or ion is present in solution is referred to as its speciation . For example, uranium can be present in a variety of species including U^{5+}, U^{6+}, UO_2^{+2}, $UO_2CO_3^0$, and UO_2OH^+. As stated previously, the speciation of an ion or molecule affects its reactivity and, therefore, its transport in the subsurface environment.

The basic idea behind surface complexation modeling is to treat the mineral or soil surface as another component, like an ion or molecule, capable of reacting with other components in solution to form a variety of species (e.g., sorbed with a metal ion, protonated or deprotonated form of the mineral surface).

Mathematical modeling using a thermodynamic equilibrium approach has been employed in this study to predict the speciation of uranium and other metals/radionuclides. While this approach is valid for both aqueous-phase and surface-sorption speciation modeling, the empirical nature of metal/radionuclide sorption data necessitate that stability constants be developed on a site-by-site basis. This is due to the fact that the adsorbent phases (i.e., mineral and soil surfaces) are often a mixture of materials and their compositions and chemical characteristics vary significantly from site to site. For these reasons, aqueous-phase and surface-sorption speciation modeling have been analyzed separately in this study, although the influence of the aqueous phase on the solid phase, and visa versa, has been accounted for.

The thermodynamic modeling approaches used to develop this report assume that the sorption reactions in the aquifer system are fast enough that equilibrium is achieved during groundwater transport at the basins. In reality, equilibrium conditions may not be established if the groundwater velocity is fast relative to the sorption rate. Results of kinetic sorption studies of uranium to both background soils and individual minerals expected to be representative of surface coatings present in the aquifer show rapid equilibration in batch studies. This suggests that near equilibrium conditions should exist in the uppermost aquifer system at the FHSB.

3.1 Aqueous-Phase Speciation Modeling

MINTEQA2 (Allison et al. 1991), the U. S. Environmental Protection Agency's geochemical equilibrium speciation model, was used to estimate the speciation of uranium present at the site. MINTEQA2 considers the total concentrations or activities of up to 50 different components, the total ionic strength, pH, redox potential and temperature of each aqueous sample to thermodynamically calculate the species present.

Input for the model includes the total component concentrations and laboratory-derived stability constants (note: stability constants contained in the model database were used without modification). The MINTEQA2 model uses these inputs and the simultaneous solution of the nonlinear mass action and linear mass balance relationships to determine the equilibrium speciation for a system of a large number of competing chemical reactions.

For the simplified example system containing U^{5+}, U^{6+}, UO_2^{+2}, $UO_2CO_3^0$, and $UO_2(OH)^+$, the following are the mass action and mass balance equations involving uranium that require simultaneous solution:

Chemical Reaction

(a) $U^{6+} + e^- \leftrightarrow U^{5+}$ [3-1.a]

(b) $U^{6+} + O_2(g) \leftrightarrow UO_2^{2+}$ [3-1.b]

(c) $UO_2^{2+} + CO_3^{2-} \leftrightarrow UO_2CO_3^0$ [3-1.c]

(d) $UO_2^{2+} + OH^- \leftrightarrow UO_2(OH)^+$ [3-1.d]

Mass Action

$$K_a = \frac{\{U^{5+}\}}{\{U^{6+}\}\{e^-\}} \quad [3\text{-}2.a]$$

$$K_b = \frac{\{UO_2^{2+}\}}{\{U^{6+}\}\{O_2\}^{pO_2}} \quad [3\text{-}2.b]$$

$$K_c = \frac{\{UO_2CO_3^0\}}{\{UO_2^{2+}\}\{CO_3^{2-}\}} \quad [3\text{-}2.c]$$

$$K_d = \frac{\{UO_2(OH)^+\}}{\{UO_2^{2+}\}\{OH^-\}} \quad [3\text{-}2.d]$$

Mass Balance

$$U_{Total} = [U^{5+}] + [U^{6+}] + [UO_2^{2+}] + [UO_2CO_3^0] + [UO_2(OH)^+] \quad [3\text{-}3]$$

In reality, there are many more reactions involving uranium and components that can react with uranium (e.g., the carbonate system and pH). In this type of approach, all the mass action and mass balance equations must be solved simultaneously. Computer codes, like MINTEQA2, provide a convenient way to solve these complicated systems of competing chemical reactions.

3.2 Surface Sorption Modeling

The binding of a contaminant to the surface coating of a soil can be represented by the following chemical reaction:

$$\equiv (SOH_x)^{x-1} + M^z \leftrightarrow \equiv (SOH_x - M)^{(x+z-1)} \quad [3\text{-}4]$$

where: $*(SOH_x)^{(x-1)}$ represents the soil surface coating which may be protonated, deprotonated or neutrally charged;
x is the number of protons associated with a binding site;
M is a metal ion with charge z; and
$*(SOH_x\text{-}M)$ is a binding site with a sorbed metal ion.

Because the reaction is assumed to be reversible, the equilibrium existing between the metal ion in solution and the metal ion sorbed may be described by an equilibrium stability constant, K, which is given by the equation:

$$K = \frac{\{\equiv (SOH_x - M)^{(x+z-1)}\}}{\{\equiv (SOH_x)^{(x-1)}\}\{M^z\}} \quad [3\text{-}5]$$

The {}'s in eqn. [3-5] represent the activity of each of the species. Activity can be related to concentration (represented by [ ]) by activity coefficients (γ) with the following equation:

$$\{\ \} = [\ ]\gamma \quad [3\text{-}6]$$

Activity coefficients correct for nonideality of solutions that arise from electrostatic interactions that occur with increasing ionic strength. For simplicity, in the remainder of this section, concentration (i.e., [ ]) will be interchangably with activity (i.e., { }). The actual models employed in this study, however, solve these equations in terms of activity and the activity coefficients are calculated based on solution ionic strength and species' properties (e.g., ion size) using classical thermodynamic approximations like the Davies and Debye-Huckel equations.

It is often assumed that an equilibrium exists between a contaminant in the aqueous phase and that sorbed on a soil surface coating. This equilibrium is described by a sorption isotherm which has the general form:

$$[M_{sorbed}] = f([M_{aqueous}]) \quad [3\text{-}7.a]$$

or

$$[\equiv (SOH_x - M^{(x+z-1)})] = f([M^z]) \quad [3\text{-}7.b]$$

where $[M_{sorbed}]$ and $[M_{aqueous}]$ are the contaminant concentrations associated with the sorbed and aqueous phase. Some factors influencing contaminant partitioning include:

the soil type (e.g., mineral surfaces present); soil binding site concentration; presence of particulate matter and colloids; contaminant concentration; competing ion concentration; and the aqueous-phase speciation of the contaminant.

Model fitting parameters generated from empirical models are generally valid only for the experimental conditions under which they were determined and, therefore, are defined as conditional stability constants. Examples of these more empirical models include the single K_d, Langmuir Isotherm, and Freundlich Isotherm models. In contrast, surface complexation models like the diffuse layer, double layer, and triple models attempt to account for the effects of changes in solution chemistry (e.g., pH and ionic strength) on binding of contaminants. The utility of these more mechanistic models is that, if working properly, these models have greater predictive power over a much wider range of geochemical conditions.

The inherent heterogeneity and geochemical variations of a real aquifer system reduces the applicability of empirical models to natural systems. This is especially true of the single K_d model (Inoue and Kaufman 1963; Van Genuchten et al. 1974; Reardon 1981) for reasons that will be discussed in the results section of this report. These considerations all impact the use of empirical partition coefficients to describe contaminant transport in natural systems. Consequently, field-scale situations or systems with a high degree of heterogeneity are usually more accurately represented as a function of these factors rather than a single constant K_d.

3.2.1 *Single K_d Model*

In the single or linear K_d model, the sorbed concentration ($[M_{sorbed}]$) is linearly related to the aqueous phase concentration ($[M_{aqueous}]$) and is defined as:

$$K_d \equiv \frac{[M_{sorbed}]}{[M_{aqueous}]} = \frac{[\equiv (SOH_x - M)^{(x+z-1)}]}{[M^z]} \qquad [3\text{-}8]$$

The slope of this equation (i.e., K_d) is always positive and is referred to as the distribution coefficient with units of l kg^{-1}. This approach assumes an infinite concentration of surface binding sites ($*SOH_x^{(x-1)}$) and is, therefore, valid only under conditions of low surface loading and low aqueous contaminant concentration.

3.2.2 *Langmuir Models*

One model that attempts to account for the finite number of sorption sites that exist on a sorbent surface is the Langmuir one-site model. This model accounts for the reduced sorption that is predicted as a greater number of binding sites become occupied under conditions of increased aqueous contaminant concentration. The one-site Langmuir equation is:

$$\left[M_{sorbed}\right] = \frac{\left[\equiv SOH_x^{(x-1)}\right]_{Total} K_{lang}\left[M^z\right]}{1 + K_{lang}\left[M^z\right]} \quad [3\text{-}9]$$

where K_{lang} is the stability constant, $[*SOH_X^{(x-1)}]_{Total}$ is the binding site concentration, and M is the contaminant with a charge of z. The Langmuir isotherm assumes a single type of binding site, no interactions between sorbed molecules, and a uniform site density.

When considering a surface with two distinct types of binding sites or mechanisms, a two site Langmuir model can be employed (Stumm 1992). This model is implemented by the addition of a second class of binding site to eqn. [3-9].

$$\left[M_{sorbed}\right] = \frac{\left[\equiv SOH_x^{(x-1)}\right]_{Type\text{-}11} K_{lang\text{-}1}\left[M^z\right]}{1 + K_{lang\text{-}1}\left[M^z\right]} + \frac{\left[\equiv SOH_x^{(x-1)}\right]_{Type\text{-}2} K_{lang\text{-}2}\left[M^z\right]}{1 + K_{lang\text{-}2}\left[M^z\right]} \quad [3\text{-}9.a]$$

3.2.3 *Electrostatic Surface Complexation Models*

Surface complexation models, which consider the electrostatic effects at the molecular level, may also be used to model contaminant sorption. In these models, both the influence of the permanent charge associated with the soil on the ions in solution, and the affect of the ions in solution on the surface charge due to sorption are considered. Two surface complexation models, the diffuse-layer model and the constant capacitance model, will be used in this work. Details of a third model, the triple-layer model, will also be discussed. The surface complexation models implemented in this work do not take full advantage of the models usefulness as the effects of all competing ions in solution will not be considered. The variable charge models which are introduced, do consider the competing effect of the H^+ ions on sorption.

3.2.3.1 Diffuse-Layer Model

The diffuse-layer model is designed for oxide surfaces. It assumes that the total charge associated with a soil can be described using two charged layers. The inner layer contains binding sites which may specifically adsorb ions such as H^+, OH^- or trace metal ions and complexes from solution. It is represented by three distinct types of binding sites on the soil surface: protonated (SOH_2^+), deprotonated (SO^-), or neutral (SOH^0 or SOM^0) sites. The second, or diffuse, layer is comprised of non-specifically sorbed ions attracted to the charge of the first layer. The total effective charge of the soil surface (σ_{tot}) is a function of the permanent charge of the soil caused by the substitution of atoms (σ_0, units of C m^{-2}), the charge of sorbed H^+ and OH^- ions, and the charge of non-specifically sorbed anions and cations in the diffuse layer (σ_d). Under typical conditions the permanent soil charge is negative as +1, +2 and +3 valence atoms replace +4 valence silicon atoms in the soil matrix. The total charge of the inner layer is balanced by that of a diffuse layer.

The effective potential of the soil surface (ψ_{tot}, units of V) can be described using Gouy-Chapman theory. It treats each ion as point charges which interact with each other only through electrostatic forces. The diffuse-layer equation derived from this theory (Stumm and Morgan 1981) is

$$\psi_{tot} = \frac{2RT}{ZF}\sinh^{-1}\left\{\frac{\sigma_{tot}}{\sqrt{8RT\varepsilon\varepsilon_0 I*10^{-3}}}\right\} \qquad [3\text{-}10.a]$$

where: R is the gas constant (8.314 J mol^{-1} K^{-1});
T is the absolute temperate (K);
Z is the effective ionic charge of the groundwater (assumed equal to 1);
F is Faraday's constant (96490 C mol^{-1});
ε is the relative dielectric permittivity in water (78.5 at 25 °C);
ε_0 is the permittivity in a vacuum (8.854 x 10^{-12} C^2 J^{-1} m^{-1}); and
I is the ionic strength of the groundwater

Assuming low surface potential (ψ_{tot} < 25 mV) and solution temperature of 25 °C, eqn. [3-10] may be simplified to

$$\psi_{tot} = 0.051\ \sinh^{-1}\left(\frac{\sigma_{tot}}{0.1174* I^{\frac{1}{2}}}\right) \qquad [3\text{-}10.b]$$

Because the electrostatic potential between the surface and the ions in solution influences the activity of the ions, exponential Boltzmann terms must be introduced into the equilibrium equation to account for the energy required to attract an ion to the soil surface. Using the diffuse layer model, the equilibrium constant for the reaction in eqn. [3-4] may be described by the equation:

$$K_{dlm} = \frac{\{\equiv (SOH_x - M)^{(x+z-1)}\}}{\{\equiv SOH_x^{(x-1)}\}_{Total}[e^{-\frac{\psi_{tot}F}{RT}}]^{(x-1)}\{M^z\}[e^{-\frac{\psi_{tot}F}{RT}}]^z} \qquad [3\text{-}11]$$

The Boltzmann terms in the denominator account for the charges of the surface (x-1) and of the metal ions (z). Note that since the surface charge is of opposite polarity to the metal ion charge, its associated Boltzmann term may be written in the numerator of the equation with an reversed exponent (positive instead of negative). This allows the diffuse layer model equation to be reduced to:

$$K_{dlm} = \frac{\{\equiv (SOH_x - M)^{(x+z-1)}\}}{\{\equiv SOH_x^{(x-1)}\}_{Total}\{M^z\}[e^{-\frac{\psi_{tot}F}{RT}}]^{(x+z-1)}} \qquad [3\text{-}12]$$

To allow for a better estimate of the accumulation of H^+ ions on the soil surface, a variable charge diffuse-layer model was designed which allowed charge to vary with the pH of the bulk groundwater. The concentration of H^+ ions near the surface soil is a function of the permanent charge of the soil and bulk solution pH and may be estimated by the following equation (Stumm and Morgan 1981)

$$pH_{surface} = pH_{bulk} + \frac{F\psi_0}{2.3RT} \qquad [3\text{-}13]$$

where ψ_0 is the potential associated with the soil surface (no diffuse layer) and is estimated based on the percent atomic substitution in the soil matrix and the surface area of the soil.

For the purposes of modeling, the entire Boltzmann factor term was treated as a model fitting parameter (Y). The corrected charge associated with the surface (σ_{cor}) can then be given by:

$$\sigma_{cor} = \sigma_0 + 10^{-(pH_{Bulk}-Y)} \qquad [3\text{-}14]$$

and may be substituted for σ_{tot} in eqn. [3-12].

3.2.3.2 Constant Capacitance Model

A simplified case of the diffuse layer model is the constant capacitance model in which the surface potential decreases linearly with respect to distance. The effective surface potential is equal to the total soil charge divided by the capacitance between the soil surface and the diffuse layer (c in units of F). The capacitance value is a function of the soil charge, the permittivity of the water, and the thickness of the diffuse layer which is related to ionic strength. In this work the effective surface potential will be estimated using a further approximation of eqn. [3-10.a] (Stumm and Morgan 1981):

$$\psi_{tot} \cong \frac{\sigma_0}{2.3\sqrt{I}} \qquad [3\text{-}10.c]$$

where the denominator is the effective capacitance. Equation [3-12] is used to calculate an equilibrium constant (K_{ccm}) using the constant capacitance model.

3.2.3.3 Triple-Layer Model

The triple-layer model (Davis and Leckie 1978) is also designed to model oxide surfaces. Like the diffuse-layer model, sorption sites on the inner most layer may protonate or deprotonate, but do not specifically adsorb trace metal ions or complexes from solution. These ions and complexes are considered to be in the second plane. The third plane is the diffuse layer and accounts for ions electrostatically attracted to, but not sorbed, to the surface. This model requires three Boltzmann factors, one for the charge associated with each layer, and a surface potential term for each of the two inner layers. Again,

considering the reaction in eqn. [3-4], the equilibrium constant using this model is given by:

$$K_{tlm} = \frac{\{\equiv (SOH_x - M)^{(x+z-1)}\}}{\{\equiv SOH_x^{(x-1)}\}_{Total}[e^{\frac{\psi_1 F}{RT}}]^{(x-1)}\{M^z\}[e^{\frac{\psi_2 F}{RT}}]^z} \quad [3\text{-}15]$$

where ψ_1 and ψ_2 are the potentials of the surface layer and the specifically adsorbed ion layer respectively.

When using surface complexation models, one must consider a number of variables. These include the equilibrium constants for protonation and deprotonation of the inner layer binding sites; the equilibrium constants for reactions between the species of interest and the protonated, deprotonated, and neutral sites; the capacitance between layers; and the activities of available binding sites and aqueous phase ions of interest. The triple-layer model usually provides a better fit of observed data than either the diffuse-layer or constant capacitance models. It has been suggested that this is due more to the increased number of fitting parameters rather than a better description of actual surface sorption phenomena (Hayes 1990).

4.0 RESULTS

4.1 Aqueous Sample Geochemistry

Aqueous samples obtained in this study spanned a wide range of geochemical conditions. Sample pH varied from 3.1 and 7.1, while Eh values were between +41 and +442 mV. All samples typically had high nitrate and ^{3}H concentrations. Nitrate levels varied from 3.9 to 1600 mg l^{-1}. ^{3}H levels ranged between 180 and $1.12x10^{6}$ Bq l^{-1}. The major cations in the samples included Al^{3+}, Fe^{3+}, K^{+}, Mg^{2+}, and Na^{+}. Although not specifically analyzed for, $HSiO_4$ is expected to be present as a major cation. The major ion chemistry is consistent with the addition of large amounts of nitric acid to the system and the dissolution of both clay minerals (e.g., kaolinite) and existing surface mineral coatings (e.g., iron (oxy)hydroxides). Typical ionic strength of the samples was approximately $1x10^{-1}$ mol l^{-1}. Conductivities varied widely, and were inversely correlated with pH. At low pH values, where the effects of the contaminant plume were most obvious with conductivities between 5 and 35 S m^{-2}. Aqueous samples with minimal impact had typical conductivities of less than 3 S m^{-2}. Aqueous inorganic carbon content was found to be < 1 mg l^{-1} in all samples.

As a result of basin operations, uranium contamination of the groundwater downgradient from the seepage basins has been observed. Aqueous concentrations of ^{238}U are reported above ICP/MS detection limits for 48 of 56 water samples in Tables 4-1 to 4-7. Concentrations vary from 0.082 µg L^{-1} ($1.0x10^{-3}$ Bq l^{-1}) to 3200 µg l^{-1} (40 Bq l^{-1}). Aqueous ^{235}U concentrations were observed above ICP/MS detection limits in 26 of 56 analyzed water samples (all in F-Area) and found to vary from 0.040 µg l^{-1} ($3.2x10^{-3}$ Bq l^{-1}) to 14 µg l^{-1} (1.1 Bq l^{-1}). Aqueous concentrations of ^{235}U are reported in Tables 4-8 to 4-14.

4.2 Soil Geochemistry

4.2.1 *Particle Size Distribution*

The size of the soil particles must be considered when trying to predict the binding of a contaminant to the soil. In situations where the controlling reactive binding sites are present in the form of surface mineral coatings, the number of potential contaminant binding sites on the soil is directly related to the surface area of the particles. Surface area is an inverse cubic function of the radius of the soil particles. One gram of clay particles will have as much as a million times more surface area, and potential binding sites, than the same weight of larger diameter sand particles.

Using the USDA soil classification scheme (Soil Survey Staff, 1975), the subsurface soils downgradient of FHSB examined in this study are sands, loamy sands, and sandy loams. A listing of the sand, silt, and clay fraction of each sample is included in Tables 4-15 to 4-20. Samples from F-Area were sands and loamy sands. Sand content varied from 73 - >99%. Silt and clay contents were 0 -12 and 0.5 - 22% respectively. H-Area samples

typically had a higher clay content than F-Area samples and can be generally classified as sandy loams or loamy sands. Sand content in H-Area samples was between 57 and 94%. The silt and clay fractions of the samples was 0 -10% and 2-42% respectively.

4.2.2 *Cation Exchange Capacity*

The cation exchange capacity (CEC) of a soil is a measure of the quantity of readily exchangeable cations present in the soil. CEC is generally highly correlated with the clay content of the soil and, mechanistically, is often thought of as the quantity of clay inner layer binding sites capable of undergoing exchange reactions. In reality, analytical techniques used to quantify CEC measure both these inner layer exchange sites as well as probably some weaker exchange sites associated with the outer surface of the mineral matrix. CEC can be used to estimate how easily a positively charged groundwater contaminant can replace the cations which naturally are associated with the soil surface.

The CEC of the soils analyzed in this work were relatively low. This is probably due to the high percentage of sand in the F- and H-Area soils. Sand, being of larger radius than silt or clay, has less surface area available to undergo ion exchange and contains no inner layer exchange binding sites that are present in clays. Samples with a higher fraction of clay and silt, have more surface area and inner layer exchange sites available for ion exchange, and therefore a higher CEC. The CEC for the soils examined in this study are listed in Tables 4-15 to 4-20. The CEC was found to vary from <1 - 29 meq kg^{-1}. There is a direct correlation between the clay fraction of the soil and the CEC.

4.2.3 *Uranium*

Soil concentrations of ^{238}U were above ICP/MS detection limits for 83 of the 84 samples and are summarized in Tables 4-1 to 4-7. Concentration of ^{238}U varied from 0.51 $\mu g\ g^{-1}$ (6.4 Bq kg^{-1}) to 19 $\mu g\ g^{-1}$ (236 Bq kg^{-1}) with an average concentration of 3.5 ± 2.8 $\mu g\ g^{-1}$. ^{235}U was present at detectable concentrations in 75 of 84 samples. ^{235}U concentrations are reported in Tables 4-8 to 4-14. Concentration of ^{235}U in these samples was observed to vary from 3.5×10^{-3} $\mu g\ g^{-1}$ (0.28 Bq kg^{-1}) to 0.11 $\mu g\ g^{-1}$ (8.8 Bq kg^{-1}) with an average concentration of 0.027 ± 0.012 $\mu g\ g^{-1}$.

4.3 Isotopic Ratios For Uranium

Natural uranium exists as three isotopes. The primary isotope is ^{238}U which makes up 99.275% of all natural uranium. ^{235}U, the fissionable isotope of uranium, represents 0.720% of all natural uranium. Based on the abundances of these two isotopes the ratio of ^{235}U atoms to ^{238}U atoms in a natural sample should be 0.00725. The third isotope, ^{234}U, exists as a product of ^{238}U decay and is only 0.005% of naturally occurring uranium. Because of its low abundance, ^{234}U was not examined in this work.

To sustain a fission process, uranium must be enriched with respect to the percentage of ^{235}U in natural samples. Depending on the reactor design, this enrichment may vary from

3 to >95 percent ^{235}U. Once the fuel is involved in a nuclear reaction, the percent enrichment of ^{235}U decreases as a many more atoms of ^{235}U undergo thermal fission when compared with ^{238}U. In many other applications, depleted uranium, a by-product of U^{235} enrichment of natural uranium, is used.

In the separations areas at SRS, two distinct processes involving uranium occurred. F-Area was involved with the separation of actinides from irradiated targets which were made of depleted uranium. In H-Area, spent fuel elements were dissolved for reprocessing. Although it had undergone fission, the uranium in these rods was still enriched in ^{235}U with respect to natural uranium.

The isotopic ratios of uranium observed downgradient of the FHSB reflect the processing activities that took place in the respective area. Both the aqueous and soil samples from F-Area show that the uranium is depleted with respect to natural uranium. Of the 33 aqueous samples from that area, 25 have both ^{235}U and ^{238}U concentrations above the ICP-MS detection limit (see Figure 4-1). The average isotopic ratio is 0.0049±0.0017. This depletion is even more noticeable in the 10 samples from the 'A' and 'D' transects near basin F3. The average isotopic ratio in those transects is 0.0032±0.00078. Figure 4-2 shows the isotopic ratio for the 47 of the 56 soil samples from F-Area with both isotopes above the analytical detection limit. The average isotopic composition of these samples was 0.0059±0.0016. The higher ratio detected in the soil is likely a result of considering the higher natural uranium content in the soil matrix measured as a result of total digestion of the soil sample.

Aqueous uranium concentrations in H-Area were much lower than those in F-Area. As a result, ^{235}U was less than the lower detection limit in all samples and no isotopic ratio can be reported for the aqueous phase samples. Many of the soil samples from H-Area were found to be enriched in ^{235}U. In the soil, reportable concentration of both isotopes were available in 27 of the 32 samples. Figure 4-3 shows the ratio of ^{235}U to ^{238}U in each of the soil samples. These samples had an average isotopic ratio of 0.0081±0.0023. The greatest enrichment could be seen in the vadose zone samples nearest the basins.

4.4 Aqueous-Phase Speciation

Using MINTEQA2, a pH-Eh stability diagram was constructed for uranium based on the geochemical conditions observed in a representative porewater sample (sample B24) and a range of pH between 0 and 8 and Eh between -300 and +500 mV (Figure 4-4). The major ion chemistry for this sample, which was used as input data for the modeling run, is listed in Table 4-21. Also plotted on this stability diagram are the pH and Eh of the other porewater samples. From this analysis, the uranium species anticipated in the groundwater downgradient of the FHSB are UO_2^+, UO_2^{2+}, UO_2OH^+, and $UO_2CO_3^0$. This is very similar to the theoretical speciation of a system containing 10^{-6} M U and 10^{-2} atm CO_2 reported by Langmuir (1979). The majority of the porewater samples collected in this work the groundwater chemistry are in the pH-Eh range where UO_2^{2+} is predicted to be the dominant form of uranium in the aqueous phase.

The charge of the aqueous-phase uranium species will have a large influence on binding to soil surfaces, with the neutral and negatively charged species tending to be more mobile. Because the geochemistry of the system is expected to change during remediation, the influence of these changes on the speciation, and ultimately the transport of uranium species, were examined in this modeling exercise. From the chemical speciation modeling conducted for a typical porewater sample, described above, and a literature review it is anticipated that changes in redox potential, pH, and carbonate content will have the greatest influence on uranium speciation during remediation. Speciation modeling has been conducted to simulate the changes that may occur during remediation. These are discussed below.

4.4.1 *Influence of Redox Potential and pH*

In the environment, uranium can exist is oxidation states of 4+, 5+, and 6+ (i.e., U(IV), U(V), and U(VI)). The generalized reaction for the U(V)/U(VI) redox couple has been presented in Equation 3-1.a. The redox potentials (Eh), a measure of the electron activity, of porewater samples were measured in the field using a platinum electrode. For the samples collected in this study, Eh values ranged from +41 to +442 mV with an average of 252 ± 101 mV (see Figure 4-4).

The effect of pH (i.e., hydrogen ion activity) on aqueous uranium speciation is primarily from the hydrolysis of uranium ion as represented by eqn. [3-1.d]. At higher pH values these uranium hydroxide species often precipitate from solution. The average pH values for the porewater samples collected in this study (calculated as -log(average of hydrogen ion activity)) was 3.70 with a range of between 3.1 and 7.1 (see Figure 4-4).

The influence of redox potential and pH on uranium speciation in these waters was evaluated by conducting model runs using MINTEQA2 for a simple system containing uranium (IV), (V), and (VI) with a total uranium concentration of 1 mg/L at pH values between 3 and 7.75 and Eh values of 50, 300, and 500 mV. The results of these modeling runs are presented in Figures 4-5 to 4-7. Under the more reducing conditions of an Eh value of 50 mV, practically all the uranium is predicted to precipitate as the U(IV) solid amorphous UO_2 (see Figure 4-5). For the two higher Eh values of 300 and 500 mV (see Figures 4-6 and 4-7), at pH values below 6.75 the system is dominated by aqueous U(VI) in the form UO_2^{2+}. At pH values at or above 6.75, uranium is predicted to precipitate from solution as the U(VI) hydroxide mineral schoepite ($UO_2(OH)_2$).

During remediation, when groundwater is brought to the surface, it is anticipated that the waters will become more oxidizing. This is expected to favor the formation of soluble U(VI) species. Also during remediation, the pH of the treated water is expected to increase. The pH increase is not expected to be in the range (i.e., >pH=6.75) where significant uranium precipitation is expected to occur. Therefore, over the pH range anticipated during remediation, the aqueous-phase speciation of uranium is predicted to be largely unaffected by changes in the hydrogen ion activity (i.e., pH).

4.4.2 *Carbonate Complexation*

Over the range of geochemical conditions expected at the FHSB the chemical reaction of the carbonate anion with the uranyl ion (see eqn. [3-1.c]) is expected to be the dominant uranium carbonate complex. The dicarbonate complex is predicted to be present, but is unimportant at pH values less than seven.

Inorganic carbon (i.e., carbonate) is expected to be added to groundwaters downgradient of the FHSB during remediation by the following mechanisms or pathways: (1) as limestone placed in the basins dissolves and is transported to the groundwater; (2) as groundwater is brought to the surface for treatment and is allowed to equilibrate with carbon dioxide in the atmosphere; and (3) as rainwater containing inorganic carbon recharges the aquifer systems. It should be noted that as the pH of the system increases, the amount of inorganic carbon (i.e., total carbonate) in a solution which is in equilibrium with the atmospheric partial pressure of CO_2 also increases (see Figure 4-8). Additionally, the speciation of the carbonate system also changes, with $H_2CO_3^0$ dominating the system at low pH values and HCO_3^- dominating at pH values above about 6.5.

As the amount of total carbonate in the system increases, so does the amount of uranium carbonate complexation for a given uranium concentration. Chemical speciation runs were made at 10^{-6} M total uranium, an Eh of 300 mV, and total carbonate concentrations of 0, 5, and 10 mg CO_3^{2-} per liter (Figures 4-9 to 4-11). While no uranium-carbonate complexes are formed in the carbonate-free system, the effect of going from five to ten mg CO_3^{2-} per liter is to reduce the pH where uranium-carbonate is the dominant uranium species from about 5.5 to about 5.25.

4.5 Uranium Partitioning

K_d values for ^{235}U and ^{238}U were calculated as the ratio of soil concentration to the porewater concentration for 48 soil/porewater sample sets. Values range from 1.2 to 34,000 l kg^{-1}. Figure 4-12 shows that a marked increase in the percentage of uranium sorbed occurs above pH 4.0. It should be noted that the field derived K_d values are significantly different from the value of 40 that had been used in previous groundwater modeling and risk assessment activities.

Figure 4-13 presents the field-derived uranium K_d values versus clay fraction in the associated soil. Figure 4-14 is a plot of field-derived uranium K_d values versus the CEC of the associated soil sample. Neither of these physical soil properties are well correlated with uranium partitioning behavior. This suggests that uranium is not binding to the clays present in the aquifer by an inner layer cation exchange reaction. Rather, the data are consistent with binding to a mineral surface coating with the surface charge varying due to aqueous pH changes.

4.6 Sorption Modeling

The single K_d, Langmuir, diffuse-layer and constant capacitance models were examined with respect to their ability to fit the field observed ^{238}U partitioning data.

The adjustable parameters in each model were varied to provide the "best fit" of the data as determined by the method of least squares. In this method, difference between the actual soil concentration and that predicted by the model is calculated and squared for each data point. Model fitting parameters were adjusted until the sum of the errors squared (SES), calculated using all data points, was minimized. This may be described by the equation:

$$SES = \sum_i \left([U_{soil}]_{observed} - [U_{soil}]_{predicted} \right)^2 \qquad [4\text{-}1]$$

where: i is the number of data points; and
$[U_{soil}]_{observed}$ and $[U_{soil}]_{predicted}$ are the observed and predicted uranium concentrations associated with the soil respectively.

Using this method, relative errors associated with large concentration data points will weight more in parameter selection than errors from small concentration data points. To allow equal emphasis to be placed on the minimizing the error of each data point, a relative error should be used. This was implemented by normalizing the error squared by actual soil bound uranium concentration of that data point. Hence, eqn. [4-1] becomes

$$SES_{normalized} = \sum_i \frac{\left([U_{soil}]_{observed} - [U_{soil}]_{predicted} \right)^2}{[U_{soil}]_{observed}} \qquad [4\text{-}1.a]$$

As is reported below, this improvement does not completely remove parameter selection bias from data points with high observed concentrations.

4.6.1 *Single K_d Model*

Previous modeling efforts at the FHSB have used a constant K_d value of 40 for uranium. This implies that the uranium soil source is 40 times the aqueous concentration at a given location. Using a least squares fitting routine, it was determined that a K_d value of 3 provided a "best fit" of the observed uranium distributions. As shown in Figure 4-15, while most uranium soil concentrations are underestimated using a K_d of 3, the soil source term associated with very high aqueous concentrations is overestimated.

4.6.2 *Langmuir Models*

The Langmuir model is identical to the single K_d model, except that it considers the existence of a finite concentration of soil binding sites. For modeling purposes, it was assumed that the soil contained a 5% clay fraction which accounted for all the available soil binding sites. The clay fraction was assumed to be all kaolinite [$Si_2Al_2O_5(OH)_4$] with a binding site density of 2.3 sites nm^{-2}. This surface area of kaolinite was measured using the BET method on a sample of pure Aiken kaolinite obtained from W R Grace & Company, Aiken, SC. It was determined to be 21.92 ±0.13 $m^2 g^{-1}$. Assuming a bulk soil density of 1.5 g cm^{-3} and an average porosity of 0.3, the binding site concentration was calculated to be $1.9x10^{-2}$ M.

Using a one-site Langmuir model, K_{lang} was calculated to be 28. Since only uranium ions were considered to be in solution, binding site saturation effects were not modeled as the total number of competing cations being considered, ant the concentration of uranium was low compared with the number of available sites. This resulted in the predicted soil concentrations being identical to those calculated with the single K_d model. It should be noted that a true Langmuir model must consider the binding of all competing ions in solution.

A two-site Langmuir model was implemented assuming 15% of the binding sites were of "Type 1" and the remaining 85% of "Type 2". Using this binding site ratio, the equilibrium constants which minimized the SES were $K_{lang-1} = 2$ and $K_{lang-2} = 114$. As in the one-site model, competition from ions other than uranium was not considered and the resulting predicted concentrations were much like the single K_d predicted concentrations.

4.6.3 *Constant Capacitance Model*

A constant capacitance model for uranium on koalinite was evaluated with a binding site concentration of $1.9x10^{-2}$ M and 0.05% substitution of silicon atoms. Since there are about 200g of kaolinite per mole, this substitution results in the soil having a permanent charge (σ_0) of -0.024 C m^{-2}. Assuming a groundwater ionic strength (I) of 1×10^{-2} and water temperature of 25°C, the surface potential associated with the diffuse layer (ψ_d) was estimated using eqn. [3-10.c] to be -0.10 V. The best fit of eqn. [3-12] to the observed field data was achieved at K_{ccm} equal to 0.55. The resulting electrostatic model provided identical results to the constant K_d model as the charge, and, therefore, the surface potential term was not allowed to vary from sample to sample.

The variable charge constant capacitance model proved to be a large improvement over the linear models. The H^+ binding fitting parameter Y in eqn. [3-14], was estimated to be approximately 1.7, but the model most closely fit the data when Y was equal to 0.5. This may be due to the H^+ ions being consider twice in the model; once in the ionic strength term in eqn. [3-10.c], and again as pH. The value K_{ccm} determined by this variable charge model was 1.2.

The predicted bound uranium concentrations of this variable charge model are shown in Figure 4-16. At aqueous uranium concentrations above 500 ppb, the model deviates substantially from the linear models. In addition to the high aqueous uranium concentration, these water samples have relatively high H^+ ion concentrations.

4.6.4 *Diffuse Layer Model*

In applying the diffuse layer model, the total ionic strength of each sample was assumed to be proportional to the field reported conductivity of the sample. Based on water sample B24, which had a conductivity of 5.0 S m^{-2} and an approximate ionic strength (as determined using MINTEQA2) of 0.0118, the relationship

$$I = \text{Conductivity (in S m}^{-2}) * 0.00236 \qquad [4\text{-}2]$$

was used to estimate total ionic strength. For several samples, no field measured conductivity is reported. For these samples, conductitivity was estimated using a known value from samples with like pH and anion chemistry. Effective surface potential was estimated using the eqn. [3-10.a].

This model "best fit" the data at K_{dlm} equal to 3.2. The predicted soil concentration was relatively good for aqueous uranium concentrations greater than 50 ppb (see Figure 4-17). As the aqueous sample concentration became lower, the error in predicted bound uranium increases, but is less than that of the linear models. In part, this may be due to the uranium in the soil matrix being a very large portion of the total uranium in the soil sample.

The double layer model was also applied using a variable surface charge model as described above. In this case the K_{dlm} was 4.4 and the value of Y was 0.5. Of all the models tested it provided the most accurate results as determined by the lowest ESE (see Figure 4-18 and Table 4-24).

4.6.5 *Empirical model*

Using the curve fitting program Sigmaplot, the fraction of uranium sorbed was fit as a function of pH. The linear, second order polynomial and third order polynomial equations were fit to the data and are shown in Figure 4-19. Coefficients associated with each of these equations are listed in Table 4-25. The third order equation provided an accurate and simplistic fit of the field-derived data.

4.7 Idealized Surface Modeling

Figure 4-20 presents experimental data for the binding of the uranyl ion to gibbsite along with the field sorption data. The gibbsite had surface area of 178.5 m^2 g^{-1}, while the total uranium concentration was 10^{-6} M (238 ppb) with no added backing electrolyte. Both data sets are in very good agreement and this is consistent with gibbsite being the dominant surface sorption surface at FHSB.

Table 4-1. ^{238}U water and soil concentrations and apparent distribution coefficients for A-transect samples (F-Area). Concentration units are ppb. K_d units are l kg^{-1}.

Sample ID	*Aqueous* ^{238}U	Std. Dev.	*Soil* ^{238}U	Std. Dev.	K_d
A11	NA		2290	69.6	NA
A12	36.5	5.58	3120	58.0	85
A13	31.4	0.92	5450	130	170
A13R	1411	41.8	7540	116	5.3
A21	NA		6630	183	NA
A22	1500	48.2	3160	107	2.1
A23	3210	56.9	5510	211	1.7
A31	2100	86.0	7770	240	3.7
A32	2990	186	4320	111	1.4
A41			3480	63.8	
A42	1130	27.6	1370	52.6	1.2
A51	NA		1940	45.6	NA
A52	0.42	0.28	932	71.9	2200
A53	232	1.33	541	35.5	2.3

NA - Vadose zone samples; no associated porewater sample or K_d.

Table 4-2. ^{238}U water and soil concentrations and apparent distribution coefficients for B-transect samples (F-Area). Concentration units are ppb. K_d units are l kg^{-1}.

Sample ID	*Aqueous* ^{238}U	Std. Dev.	*Soil* ^{238}U	Std. Dev.	K_d
B11	NA		1750	57.3	NA
B12	NA		2800	110	NA
B13	1290	19.9	3510	75.4	2.7
B14	269	5.02	2270	116	8.5
B21	NA		2260	78.6	NA
B22	NA		900	114	NA
B23	266	1.57	2690	113	10.1
B23R	520	14.1	2700	88.0	5.2
B24	562	8.71	7830	376	14
B31	NA		2660	79.0	NA
B32	13.7	6.31	5350	302	390
B33	15.8	1.37	2760	98.1	180
B41	NA		2100	79.8	NA
B42	99.2	4.41	19,100	275	190
B43	367	22.4	2350	55.6	6.4
B51	84.0	1.42	3320	158	39
B52	266	1.47	1410	61	5.3
B52R	6.13	0.64	3250	57.9	530

NA - Vadose zone samples; no associated porewater sample or K_d.

Table 4-3. ^{238}U water and soil concentrations and apparent distribution coefficients for C-transect samples (F-Area). Concentration units are ppb. K_d units are l kg^{-1}.

Sample ID	*Aqueous* ^{238}U	Std. Dev.	*Soil* ^{238}U	Std. Dev.	K_d
C11	NA		955	115	NA
C12	NA		1950	75.2	NA
C13	1310	98.8	8310	213	6.4
C14	267	2.19	6070	122	23
C21	NA		2130	305	NA
C21R	NA		2890	371	NA
C22	73.0	3.34	2170	147	30
C23	5.68	0.41	5570	126	980
C31	NA		7030	164	NA
C32	< 0.5		1810	74.3	> 3600
C33	0.547	0.004	3470	134	6300
C41	NA		1950	101	NA
C42	< 0.5		7170	83.3	> 14,000
C43	0.193	0.011	2590	121	13,000

NA - Vadose zone samples; no associated porewater sample or K_d.

Table 4-4. ^{238}U water and soil concentrations and apparent distribution coefficients for D-transect samples (F-Area). Concentration units are ppb. K_d units are l kg^{-1}.

Sample ID	Aqueous ^{238}U	Std. Dev.	Soil ^{238}U	Std. Dev.	K_d
D11	NA		1080	72.7	NA
D12	NA		9700	298	NA
D13	0.262	0.056	2830	131	11,000
D13RA	296	14.7	3930	297	13
D13RB	296	14.7	2740	170	9.3
D21	NA		1670	102	NA
D41	NA		2130	81.1	NA
D51	NA		1900	122	NA

NA - Vadose zone samples; no associated porewater sample or K_d.

Table 4-5. ^{238}U water and soil concentrations and apparent distribution coefficients for E-transect samples (H-Area). Concentration units are ppb. K_d units are l kg^{-1}.

Sample ID	Aqueous ^{238}U	Std. Dev.	Soil ^{238}U	Std. Dev.	K_d
E11	NA		4810	195	NA
E12	NA		1210	47.4	NA
E12R	NA		1160	43.8	NA
E13	6.10	0.073	1950	149	320
E14	4.49	0.148	1380	90.1	310
E21	NA		1580	109	NA
E22	NA		1810	160	NA
E23	1.17		3140	367	2700
E23R	1.77	0.062	1740	42.5	980
E24	7.80		2250	90.7	290
E31	NA		1820	61.5	NA
E32	NA		1890	151	NA
E33	1.42	0.032	2120	126	1500
E34	2.50		945	53.7	380
E41	0.278		4500	142	16,000
E42	0.176		3130	630	18,000

NA - Vadose zone samples; no associated porewater sample or K_d.

Table 4-6. ^{238}U water and soil concentrations and apparent distribution coefficients for F-transect samples (H-Area). Concentration units are ppb. K_d units are l kg^{-1}.

Sample ID	*Aqueous* ^{238}U	Std. Dev.	*Soil* ^{238}U	Std. Dev.	K_d
F11	NA		2450	52.8	NA
F12	0.526		3920	111	7500
F13	14.9		12,300	348	830
F21	NA		1020	57.4	NA
F21R	NA		505	107	NA
F22	34.0		5330	220	160
F23	0.38		6250	213	16,000
F31	NA		2940	149	NA
F32	0.294		2560	82.8	8700
F33	< 0.5		1430	102	> 2900
F41	NA		2610	171	NA
F42	0.121		4100	162	34,000
F43	10.3		3430	146	330
F51	NA		1400	88.9	NA
F52	< 0.5		2770	154	> 5500
F53	0.17		4510	267	27,000

NA - Vadose zone samples; no associated porewater sample or K_d.

Table 4-7. ^{238}U soil Concentration Data for up-gradient soil samples collected at the Little Grand Canyon (F-Area). Units are ppb.

Sample ID	*Aqueous* ^{238}U	Std. Dev.	*Soil* ^{238}U	Std. Dev.	K_d
GC4	NA		3690	152	NA
GC5	NA		1650	86.9	NA

NA - Vadose zone samples; no associated porewater sample or K_d.

Table 4-8. ^{235}U water and soil concentrations and apparent distribution coefficients for A-transect samples (F-Area). Concentration units are ppb. K_d units are l kg^{-1}.

Sample ID	*Aqueous* ^{235}U	Std. Dev.	*Soil* ^{235}U	Std. Dev.	K_d
A11	NA		17.0	4.52	NA
A12	0.116	0.032	16.1	4.15	139
A13	0.083	0.142	30.3	9.93	361
A13R	4.9	0.55	46.4	6.23	9.46
A21	NA		45.0	9.19	NA
A22	4.27	0.235	16.2	5.66	3.79
A23	11.32	0.088	17.6	7.24	1.55
A31	4.7	0.288	20.8	4.23	4.43
A32	13.87	0.531	19.1	5.34	1.38
A41			20.5	9.59	
A42	3.91	0.323	4.67	3.73	1.19
A51	NA		11.9	7.93	NA
A52	< 0.036		5.87	0.300	> 160
A53	0.847	0.308	< 13.7		< 16

NA - Vadose zone sample; no associated porewater sample or K_d.

Table 4-9. ^{235}U water and soil concentrations and apparent distribution coefficients for B-transect samples (F-Area). Concentration units are ppb. K_d units are l kg^{-1}.

Sample ID	*Aqueous* ^{235}U	Std. Dev.	*Soil* ^{235}U	Std. Dev.	K_d
B11	NA		7.63	3.38	NA
B12	NA		17.1	7.91	NA
B13	8.61	0.092	17.6	7.29	2.04
B14	1.62	0.106	16.7	3.81	10.4
B21	NA		14.9	5.49	NA
B22	NA		27.25	8.32	NA
B23	1.73	0.068	18.5	4.68	10.7
B23R	3.19	0.301	12.8	6.71	4.00
B24	3.72	0.141	42.1	10.7	11.3
B31	NA		13.3	8.74	NA
B32	0.088	0.052	29.3	7.32	332
B33	0.079	0.006	16.7	5.62	212
B41	NA		12.6	7.03	NA
B42	0.631	0.057	113	14.2	180
B43	2.43	0.171	17.3	5.32	7.12
B51	0.432	0.094	9.00	5.77	20.8
B52	1.597	0.263	4.09	2.15	2.56
B52R	< 0.036		12.1	6.37	> 180

NA - Vadose zone sample; no associated porewater sample or K_d.

Table 4-10. ^{235}U water and soil concentrations and apparent distribution coefficients for C-transect samples (F-Area). Concentration units are ppb. K_d units are l kg^{-1}.

Sample ID	*Aqueous* ^{235}U	Std. Dev.	*Soil* ^{235}U	Std. Dev.	K_d
C11	NA		< 7.73		NA
C12	NA		12.7	6.21	NA
C13	9.22	0.673	51.3	10.6	5.56
C14	1.44	0.105	40.7	7.72	28.3
C21	NA		< 58.7		NA
C21R	NA		18.0	15.0	NA
C22	0.370	0.076	10.1	6.10	27.4
C23	0.042	0.048	34.6	10.1	823
C31	NA		59.1	15.9	NA
C32	< 0.036		19.3	6.81	> 540
C33	< 0.036		24.9	7.79	> 690
C41	NA		13.5	3.97	NA
C42	< 0.036		49.4	11.0	> 1400
C43	< 0.036		16.5	10.4	> 460

NA - Vadose zone sample; no associated porewater sample or K_d.

Table 4-11. ^{235}U water and soil concentrations and apparent distribution coefficients for D-transect samples (F-Area). Concentration units are ppb. K_d units are l kg^{-1}.

Sample ID	*Aqueous* ^{235}U	Std. Dev.	*Soil* ^{235}U	Std. Dev.	K_d
D11	NA		< 50.0		NA
D12	NA		34.8	16.5	NA
D13	< 0.036		25.0	8.47	> 690
D13RA	0.613		16.3	8.19	26.6
D13RB	0.613		13.9	3.48	22.6
D21	NA		13.7	6.64	NA
D41	NA		16.3	5.09	NA
D51	NA		< 63.3		NA

NA - Vadose zone sample; no associated porewater sample or K_d.

Table 4-12. ^{235}U water and soil concentrations and apparent distribution coefficients for E-transect samples (H-Area). Concentration units are ppb. K_d units are l kg^{-1}.

Sample ID	*Aqueous* ^{235}U	Std. Dev.	*Soil* ^{235}U	Std. Dev.	K_d
E11	NA		33.2	31.6	NA
E12	NA		< 9.66		NA
E12R	NA		10.9	2.17	NA
E13	< 0.036		23.4	3.42	> 650
E14	< 0.036		7.00	3.94	> 190
E21	NA		18.6	11.6	NA
E22	NA		26.4	11.9	NA
E23	< 0.036		< 53.3		
E23R	< 0.036		11.2	3.54	> 310
E24	< 0.036		12.9	11.4	> 360
E31	NA		18.0	8.56	NA
E32	NA		16.5	10.5	NA
E33	< 0.036		16.8	7.81	> 470
E34	< 0.036		9.61	4.81	> 270
E41	< 0.036		31.4	12.3	> 870
E42	< 0.036		22.7	11.4	> 630

NA - Vadose zone sample; no associated porewater sample or K_d.

Table 4-13. ^{235}U water and soil concentrations and apparent distribution coefficients for F-transect samples (H-Area). Concentration units are ppb. K_d units are l kg^{-1}.

Sample ID	*Aqueous* ^{235}U	Std. Dev.	*Soil* ^{235}U	Std. Dev.	K_d
F11	NA		21.9	10.1	NA
F12	< 0.036		25.0	9.33	> 690
F13	< 0.036		79.2	13.4	> 2200
F21	NA		4.99	1.69	NA
F21R	NA		< 128		NA
F22	< 0.036		41.4	12.4	> 1200
F23	< 0.036		34.3	17.4	> 950
F31	NA		< 58.1		NA
F32	< 0.036		23.8	5.46	> 660
F33	< 0.036		8.00	5.95	> 220
F41	NA		20.6	5.04	NA
F42	< 0.036		32.6	9.81	> 910
F43	< 0.036		25.3	9.29	> 700
F51	NA		< 65.0		NA
F52	< 0.036		21.5	10.6	> 600
F53	< 0.036		34.5	11.9	> 960

NA - Vadose zone sample; no associated porewater sample or K_d.

Table 4-14. ^{235}U soil concentration data for background samples collected upgradient of F-Area at the Little Grand Canyon. Units are ppb.

	Aqueous		*Soil*		
Sample ID	^{235}U	Std. Dev.	^{235}U	Std. Dev.	K_d
GC4	NA		33.74	4.03	NA
GC5	NA		< 49.5		NA

NA - Vadose zone sample; no associated porewater sample or K_d.

Table 4-15. Chemical and physical properties of water and soil samples in the A-transect (F-Area).

Sample ID	*Aqueous* pH	Eh (mV)	TIC (ppm)	TOC (ppm)	*Soil* % Sand	% Silt	% Clay	CEC (meq kg^{-1})	CEC Std. Dev.
A11	NA	NA	NA	NA	88.3	2.7	9.0	9.97	0.14
A12	4.16	287	<1	3.5	99.5	0	0.5	1.11	0.16
A13*	4.99	41.3	<1	13	95.0	1.6	3.3	1.82	0.20
A13R	3.42		<1	2.4	93.6	3.4	3.0	3.74	0.16
A21	NA	NA	NA	NA	89.9	5.1	5.0	5.94	0.17
A22	3.19	378	<1	14	95.7	2.8	1.5	1.39	0.16
A23	3.01	442.1	<1	8	95.3	0.2	4.5	1.40	0.17
A31	3.19	345.2	<1	14	95.6	0	4.4	7.92	0.17
A32	3.5	428.9	<1	10	89.5	7.4	3.1	<1	
A41	4.8	186.8	<1	2	92.2	2.9	4.9	4.03	0.20
A42	3.29	404.1	<1	16	91.7	3.6	4.7	2.10	0.15
A51	NA	NA	NA	NA	76.5	10.0	13.5	12.5	0.17
A52	5.42	112	<1	6.1	92.6	4.8	2.5	0.68	0.18
A53	3.72		<1	1.7	91.7	6.3	2.0	0.42	0.18

NA - Vadose zone samples have no associated porewater samples.

* The water sample for A13 was brought to the surface using a bailer apparatus.

Table 4-16. Chemical and physical properties of water and soil samples in the B-transect (F-Area).

Sample ID	*Aqueous* pH	Eh (mV)	TIC (ppm)	TOC (ppm)	*Soil* % Sand	% Silt	% Clay	CEC (meq kg^{-1})	CEC Std. Dev.
B11	NA	NA	NA	NA	80.4	4.4	15.2	10.8	0.12
B12	NA	NA	NA	NA	89.6	4.1	6.2	11.9	0.15
B13	3.24	390.8	<1	1.8	89.6	7.6	2.8	4.71	0.15
B14	3.93	198.0	<1	2.9	93.2	3.0	3.9	3.06	0.18
B21	NA	NA	NA	NA	85.3	1.8	12.9	10.3	0.22
B22	NA	NA	NA	NA					
B23	3.86	315.3	<1	3.7	90.8	4.3	4.9		
B23R	4.02		<1	2.3	93.5	2.4	2.5	3.80	0.12
B24	3.83	315.6	<1	2.7	89.9	2.7	7.5	5.69	0.22
B31	NA	NA	NA	NA	76.7	3.9	19.4	17.3	0.17
B32	4.62	205.3	<1	3.0	92.3	1.5	6.2	2.5	0.19
B33	4.64	56.4	<1	5.1	89.2	5.3	5.5	8.42	0.198
B41	NA	NA	NA	NA	83.7	4.0	12.3	12.1	0.15
B42	4.67		<1	2.1	85.3	2.1	12.6	21.4	0.14
B43	3.66		<1	2.4	98.8	0.0	1.2	3.02	0.16
B51	4.09		<1	1.3	87.3	4.5	8.2	15.1	0.14
B52	3.61		<1	1.0					
B52R	4.69		<1	1.4	91.8	4.9	3.3	2.39	0.11

NA - Vadose zone samples have no associated porewater samples.

Table 4-17. Chemical and physical properties of water and soil samples in the C-transect (F-Area).

Sample ID	*Aqueous* pH	Eh (mV)	TIC (ppm)	TOC (ppm)	*Soil* % Sand	% Silt	% Clay	CEC (meq kg^{-1})	CEC Std. Dev.
C11	NA	NA	NA	NA	84.8	6.9	8.3	4.13	0.11
C12	NA	NA	NA	NA	80.2	5.7	14.1	13.3	0.13
C13	3.68	385.9	<1	3.7					
C14	3.75	385.8	<1	2.8	84.2	9.4	6.4		
C21	NA	NA	NA	NA	82.2	5.8	12.0	11.4	0.15
C21R	NA	NA	NA	NA	80.9	6	13.1	6.82	0.11
C22	3.96	224.9	<1	3.0				1.28	0.19
C23	4.17	280	<1	2.5	84.2	9.4	6.4	6.12	0.14
C31	NA	NA	NA	NA	93.5	1.4	5.0	5.87	0.14
C32	5.53		<1	1.7	85.7	8.8	5.5	2.54	0.12
C33	4.64		<1	2.5	85.9	8.0	6.1	8.54	0.12
C41	NA	NA	NA	NA	81.0	2.6	16.4	11.5	0.13
C42	5.27		<1	3.5	90.3	1.9	7.9	11.4	0.12
C43	4.51		<1	1.5	91.0	6.0	3.0	5.04	0.12

NA - Vadose zone samples have no associated porewater samples.

Table 4-18. Chemical and physical properties of water and soil samples in the D-transect (F-Area).

Sample ID	*Aqueous* pH	Eh (mV)	TIC (ppm)	TOC (ppm)	*Soil* % Sand	% Silt	% Clay	CEC (meq kg^{-1})	CEC Std. Dev.
D11	NA	NA	NA	NA	73.3	10.7	16	8.07	0.19
D12	NA	NA	NA	NA	83.2	6.5	10.3	4.86	0.12
D13*	6.78		<1	18.6	86.7	8	5.3	1.96	0.10
D13RA	4.14		<1	1.8					
D13RB	NA	NA	NA	NA	96.7	1.3	2.0	2.55	0.10
D21	NA	NA	NA	NA	86.1	3.2	10.7	8.96	0.14
D41	NA	NA	NA	NA	78.6	4.3	17.1	11.0	0.12
D51	NA	NA	NA	NA	86.3	3.0	10.7	12.1	0.14

* The water sample for D13 was brought to the surface using a bailer apparatus.
NA - Vadose zone samples have no associated porewater samples.

Table 4-19. Chemical and physical properties of water and soil samples in the E-transect (H-Area).

Sample ID	*Aqueous* pH	Eh (mV)	TIC (ppm)	TOC (ppm)	*Soil* % Sand	% Silt	% Clay	CEC (meq kg^{-1})	CEC Std. Dev.
E11	NA	NA	NA	NA	70.4	3.7	25.9	29.3	0.12
E12	NA	NA	NA	NA	86.4	4.4	9.2	7.42	0.09
E12R	NA	NA	NA	NA	97.9	0.0	2.1	5.05	0.10
E13	4.00	132	<1	3.0	84.6	4.9	10.5	11.4	0.08
E14	4.04	181.2	<1	2.6	94.2	1.3	4.5	8.50	0.07
E21	NA	NA	NA	NA	69.4	5.9	24.3	15.7	0.11
E22	NA	NA	NA	NA	70.8	10.1	19.1		
E23	5.85	201	<1	1.9	91.1	2.5	6.4	15.5	0.17
E23R	4.32		<1	2.4	94.4	1.7	3.9	13.3	0.11
E24	3.87	191.2	<1	2.3	87.9	4.8	7.3	13.8	0.10
E31	NA	NA	NA	NA	58.1	8.5	33.4	13.0	0.09
E32	NA	NA	NA	NA	72.6	3.2	24.2	17.3	0.11
E33	4.27	277.8	<1	1.6	90.5	3.0	6.5	11.5	0.12
E34	4.05	287.6	<1	2.8	87.2	9.1	3.7	10.5	0.12
E41	5.27	230.1	<1	1.7	66.6	1.6	31.8	20.6	0.11
E42	4.87	272.3	<1	3.7	80.2	5.3	14.5	20.6	0.17

NA - Vadose zone samples have no associated porewater samples.

Table 4-20. Chemical and physical properties of water and soil samples in the F-transect (H-Area).

Sample ID	*Aqueous* pH	Eh (mV)	TIC (ppm)	TOC (ppm)	*Soil* % Sand	% Silt	% Clay	CEC (meq kg^{-1})	CEC Std. Dev.
F11	NA	NA	NA	NA	81	5.2	13.8	14.6	0.13
F12	4.30	197.3	<1	4.6	81	3.5	15.5	16.1	0.15
F13	4.90	148.3	<1	4.2				8.51	0.17
F21	NA	NA	NA	NA	84.5	7.4	8.1	11.1	0.14
F21R	NA	NA	NA	NA	85.9	4.5	8.1	9.39	0.10
F22	4.69	224	<1	5.7	86.7	5.2	8.1	7.48	0.10
F23	6.48	255.6	<1	3.2	82.9	4.1	13	11.6	0.18
F31	NA	NA	NA	NA	61.3	5.6	33.1	14.3	0.23
F32	4.85	237	<1	3.2	82.8	2.9	14.2	15.1	0.16
F33	4.77	199.1	<1	8.5	80.7	0	18.3	13.6	0.15
F41	NA	NA	NA	NA	59.1	4.7	36.1	26.7	0.23
F42	5.20	211	<1	3.4	84.2	0	17.2	11.8	0.14
F43	4.12	176.3	<1	3.7	89.2	0	14.2		
F51	NA	NA	NA	NA	70.9	0	29.6	17.4	0.16
F52	5.91	193	<1	3.1	62.5	0	42.2	19.9	0.15
F53	5.63	221.4	<1	3.6	86.3	0	16.3	13.3	0.15

NA - Vadose zone samples have no associated porewater samples.

Table 4-21. MINTEQA2 Input Sample B24

Major Ions		Trace Metals/Radionuclides	
Componen	Conc (M)	Component	Conc (M)
Na^{+1}	3.961E-03	Cr_{Tot}	1.035E-07
Mg^{+2}	8.602E-05	Ni^{+2}	2.454E-06
Al^{+3}	1.072E-03	Cu^{+2}	5.243E-04
K^{+1}	2.610E-04	Zn^{+2}	7.730E-06
Ca^{+2}	2.496E-05	H_3AsO_4	5.407E-08
Mn^{+3}	7.176E-05	SeO_4^{-2}	1.162E-07
Fe_{Tot}	7.812E-05	Sr^{+2}	3.540E-07
CO_3^{-2}	1.144E-05	Cd^{+2}	4.228E-08
$H_4SiO_4^*$	1.236E-04	Ba^{+2}	1.056E-06
NO_3^{-1}	6.156E-03	Pb^{+2}	3.801E-07
Cl-1	2.475E-04	UO_2^{+2}	1.000E-05
SO_4^{-2}	4.271E-05		

*H_4SiO_4 concentration based concentration reported nearby well.

Table 4-22. "Best fit" model parameters and errors for observed ^{238}U contaminant partitioning.

Model	K	K_2 or Y	ESS-normalized
Single K_d	2.5	NA	6.27×10^{-4}
	40	NA	4.50×10^{-2}
Langmuir - one site	28	NA	6.27×10^{-4}
Langmuir - two site	2	114	6.27×10^{-4}
Constant Capcitance	0.55	NA	6.27×10^{-4}
- variable charge	1.2	0.5	6.03×10^{-4}
Diffuse Layer	3.2	NA	5.24×10^{-4}
- variable charge	4.4	0.5	5.18×10^{-4}

Table 4-23. Empirical model coefficients.

Fraction sorbed = $a + (b*pH) + (c*pH^2) + (d*pH^3)$

Model	a	b	c	d
Linear	0.193	0.157	0	0
Second order	-2.06	1.15	-1.05	0
Third order	-6.22	3.91	-0.698	30.04

Figure 4-1. Uranium isotopic ratio for F-Area aqueous samples.

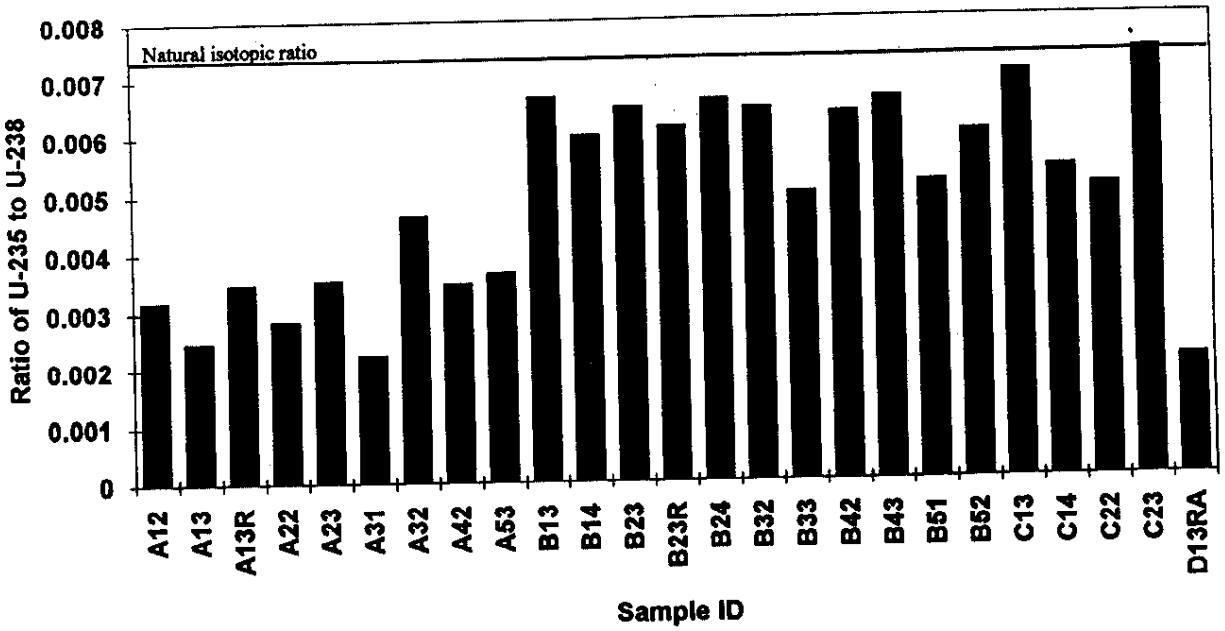

Figure 4-2. Uranium isotopic ratio for F-Area soil samples.

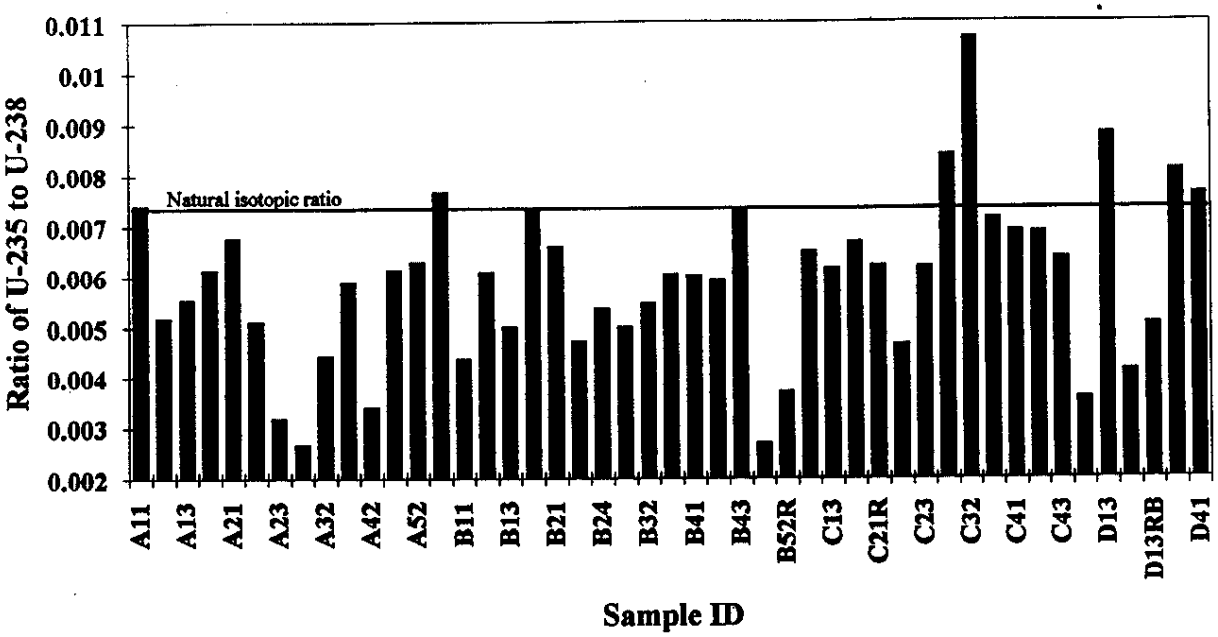

Figure 4-3. Uranium isotopic ratio for H-Area soil samples.

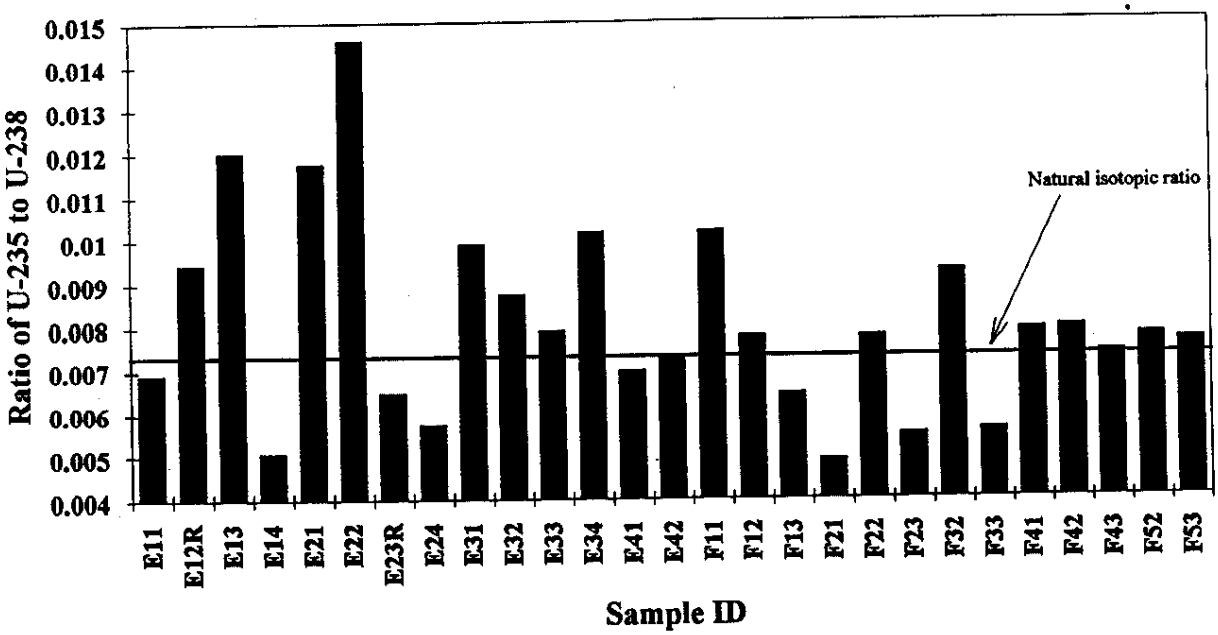

Figure 4-4. Stability diagram - Porewater sample B24

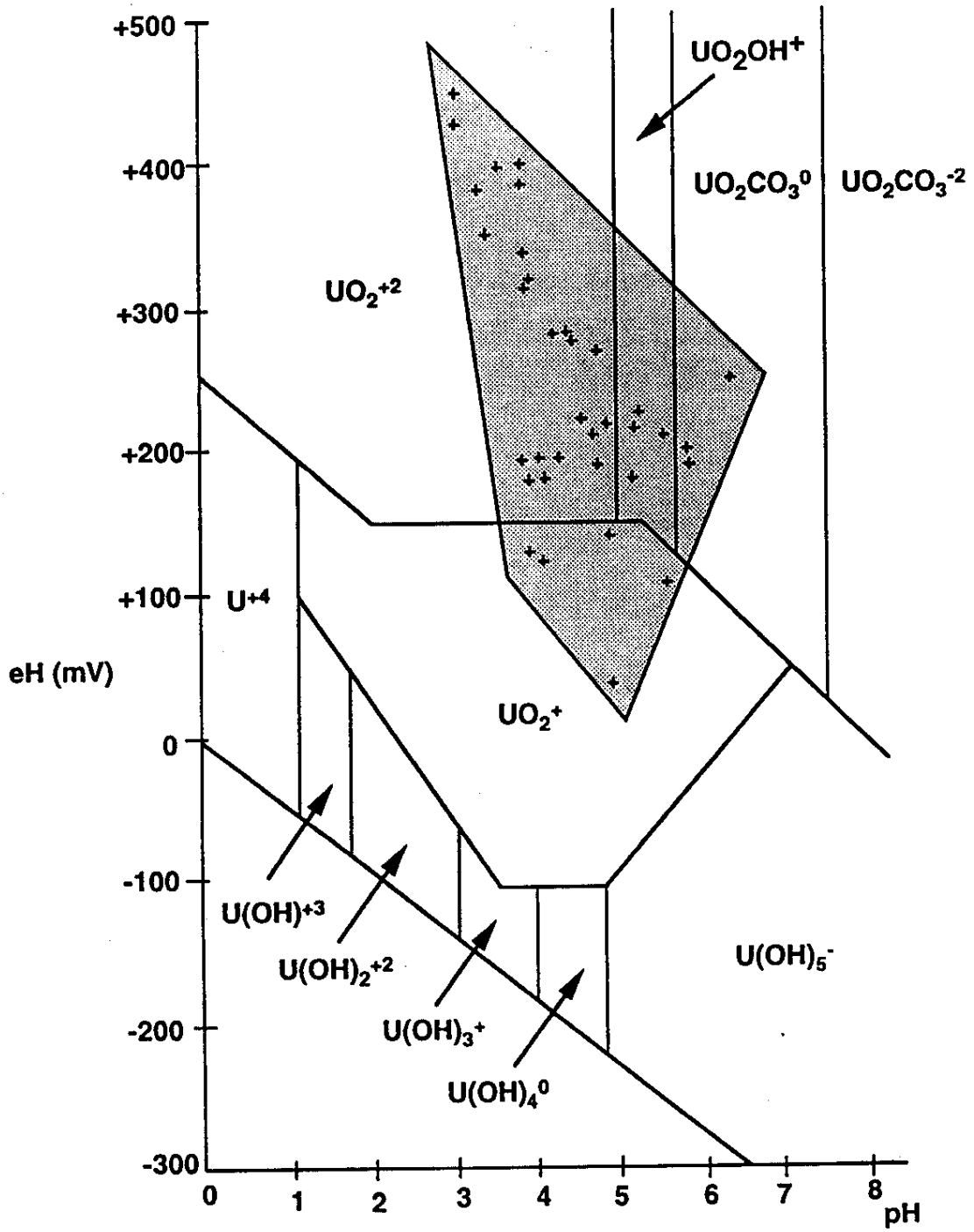

Figure 4-5. Influence of pH on uranium speciation (Redox potential = 50 mV)

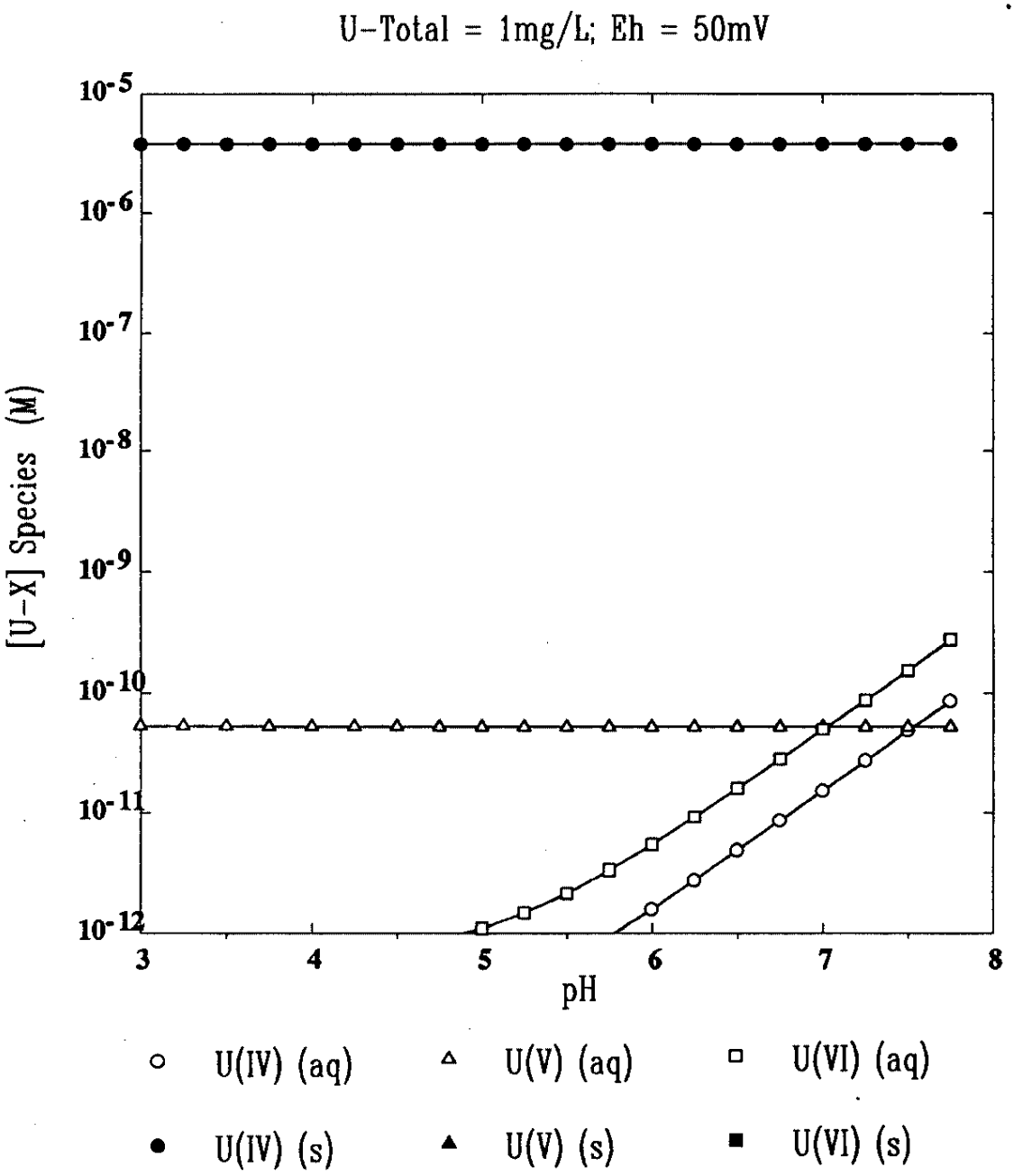

Figure 4-6. Influence of pH on uranium speciation (Redox potential = 300 mV)

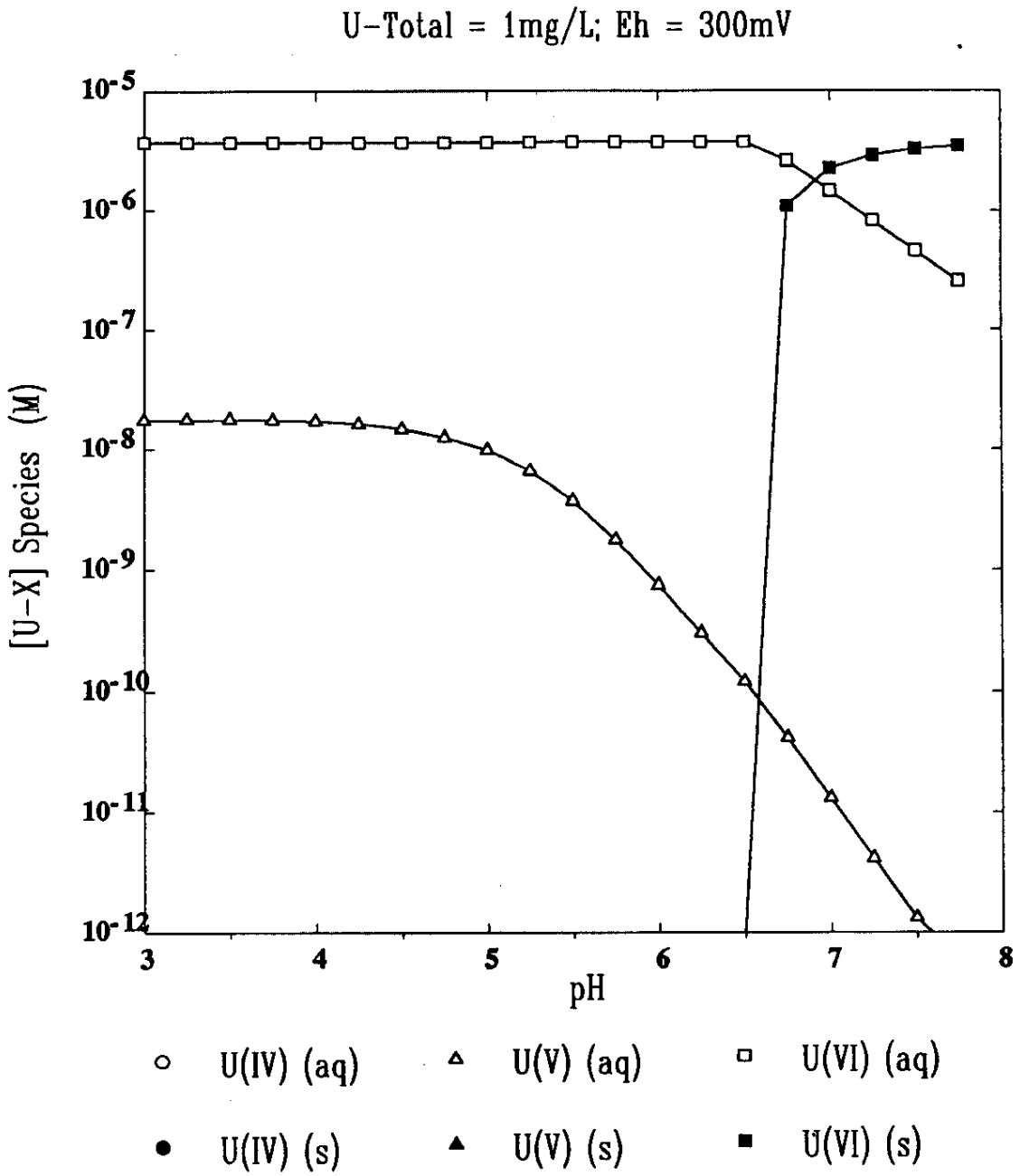

Figure 4-7. Influence of pH on uranium speciation (Redox potential = 500 mV)

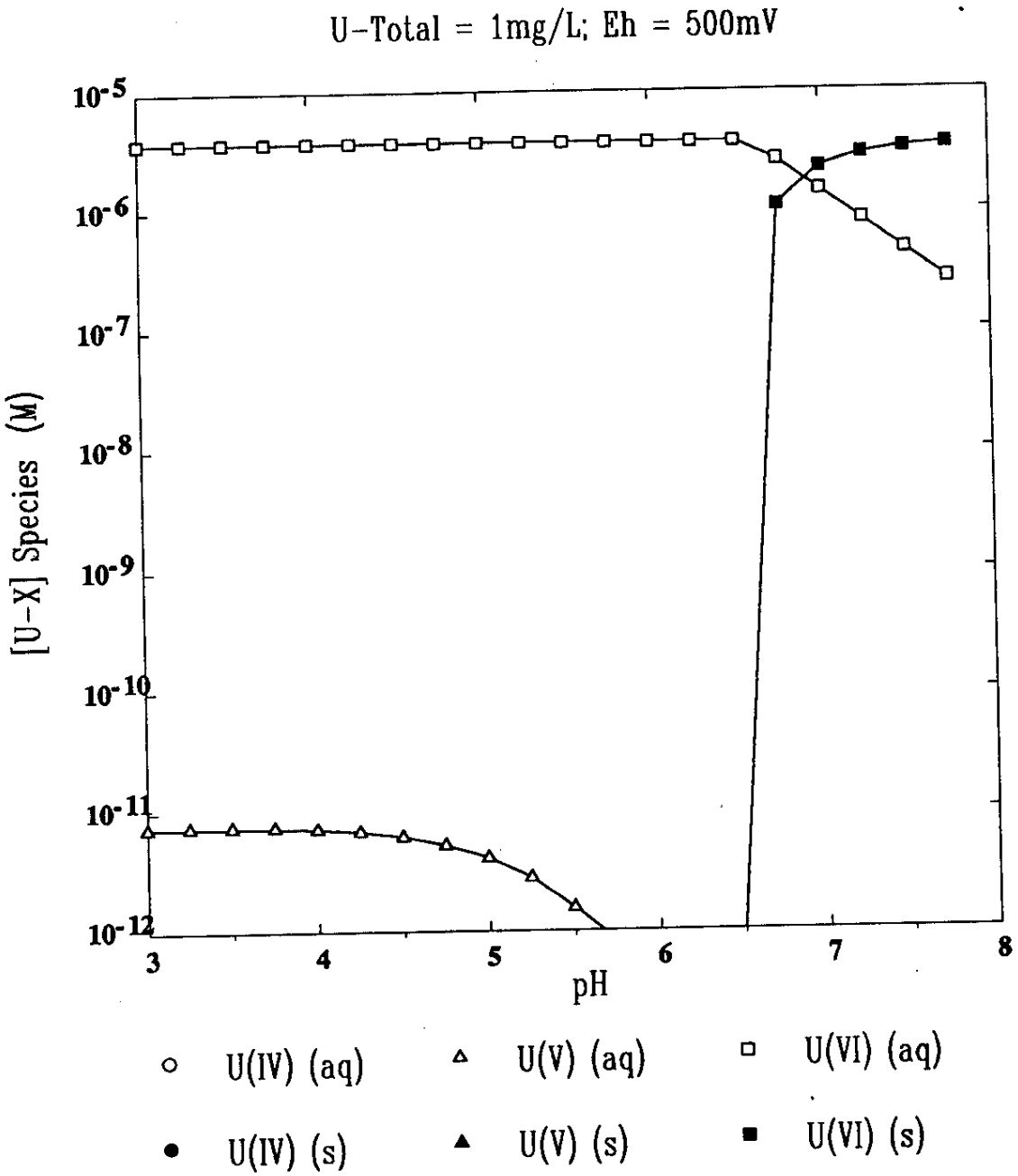

Figure 4-8. Carbonate speciation (pCO_2 = 0.003 atm.)

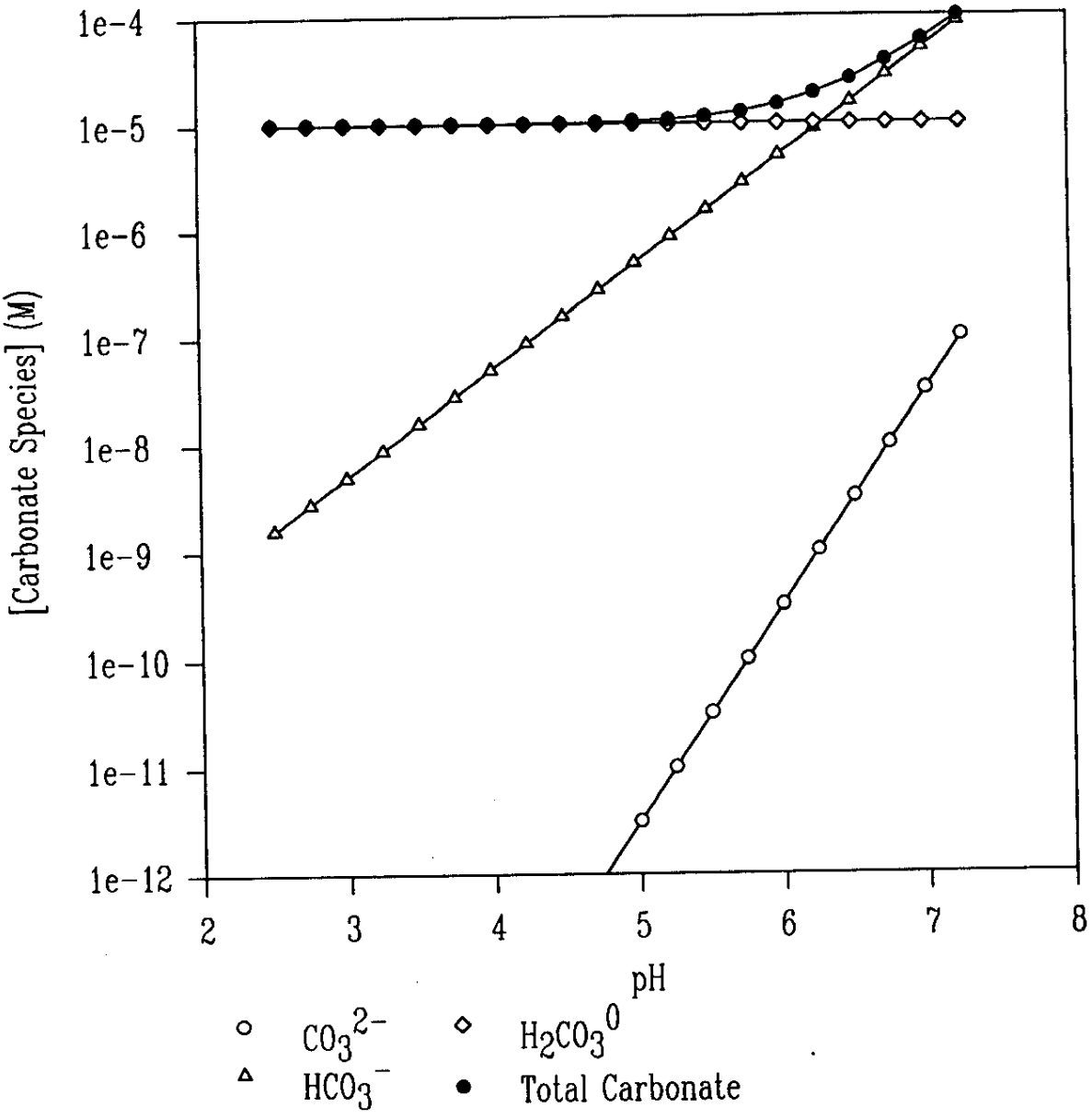

Figure 4-9. Carbonate influence of uranium speciation (CO_3^{2-} = 0 mg l^{-1})

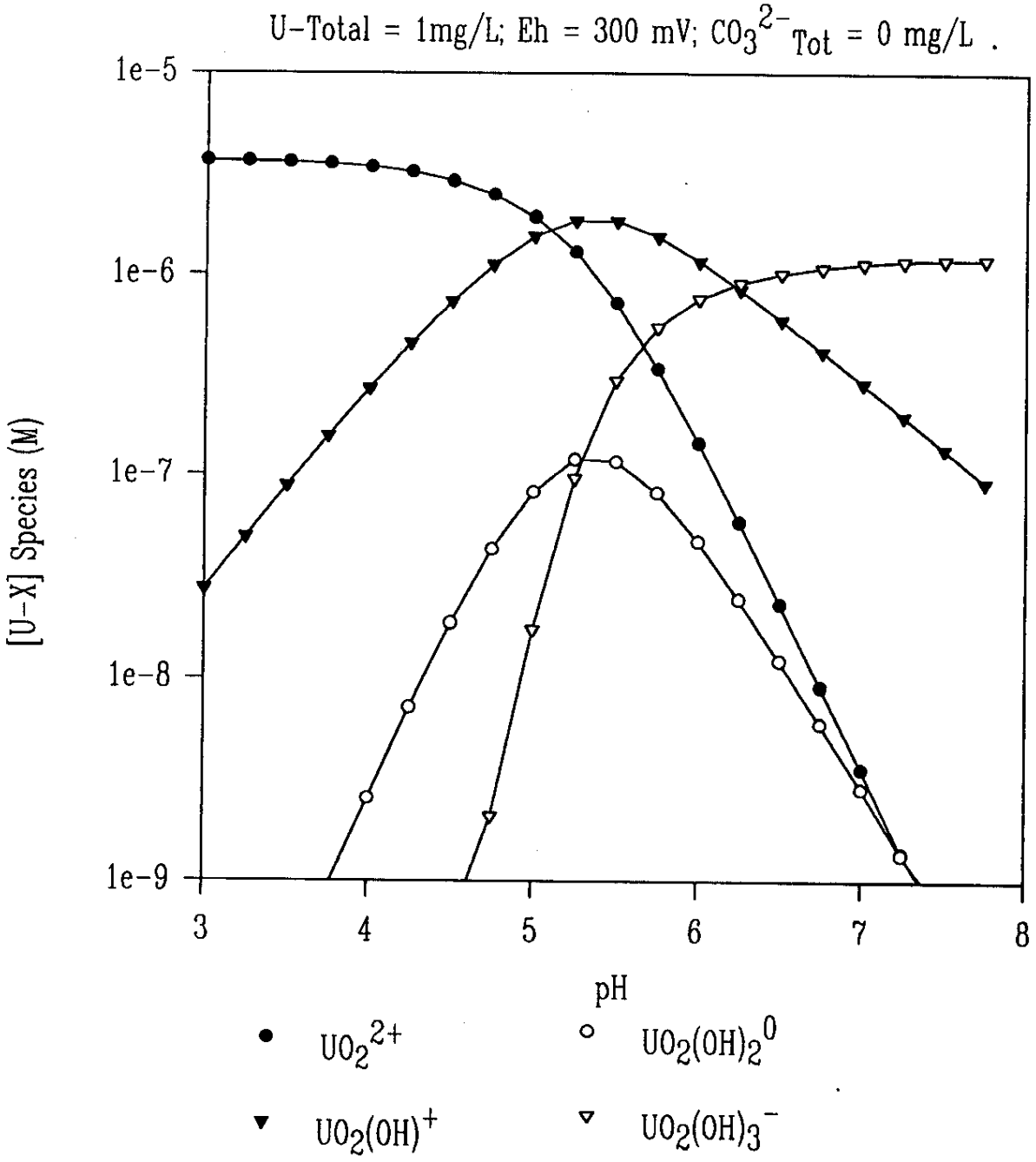

Figure 4-10. Carbonate influence of uranium speciation (CO_3^{2-} = 5 mg l^{-1})

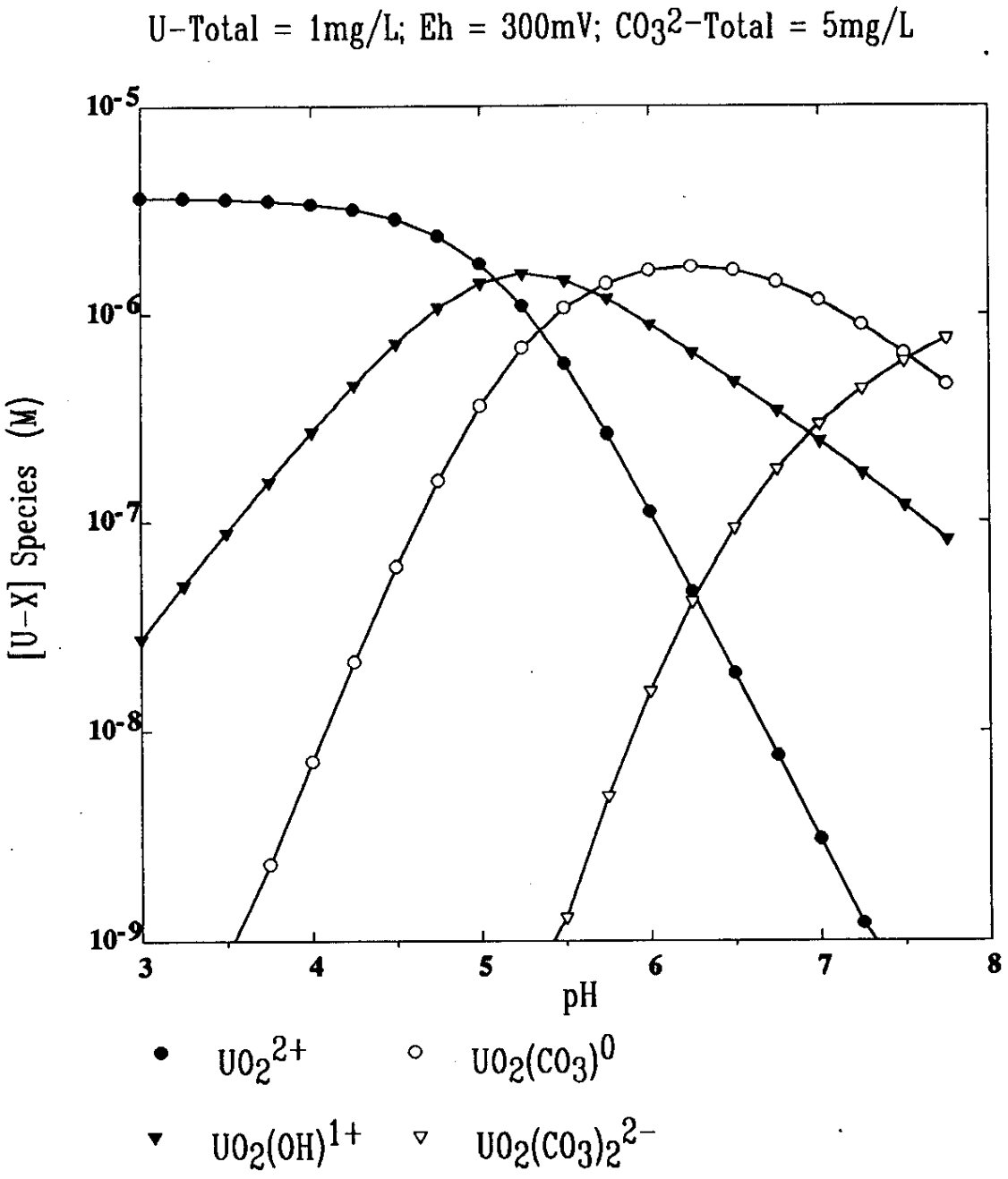

Figure 4-11. Carbonate influence of uranium speciation (CO_3^{2-} = 10 mg l^{-1})

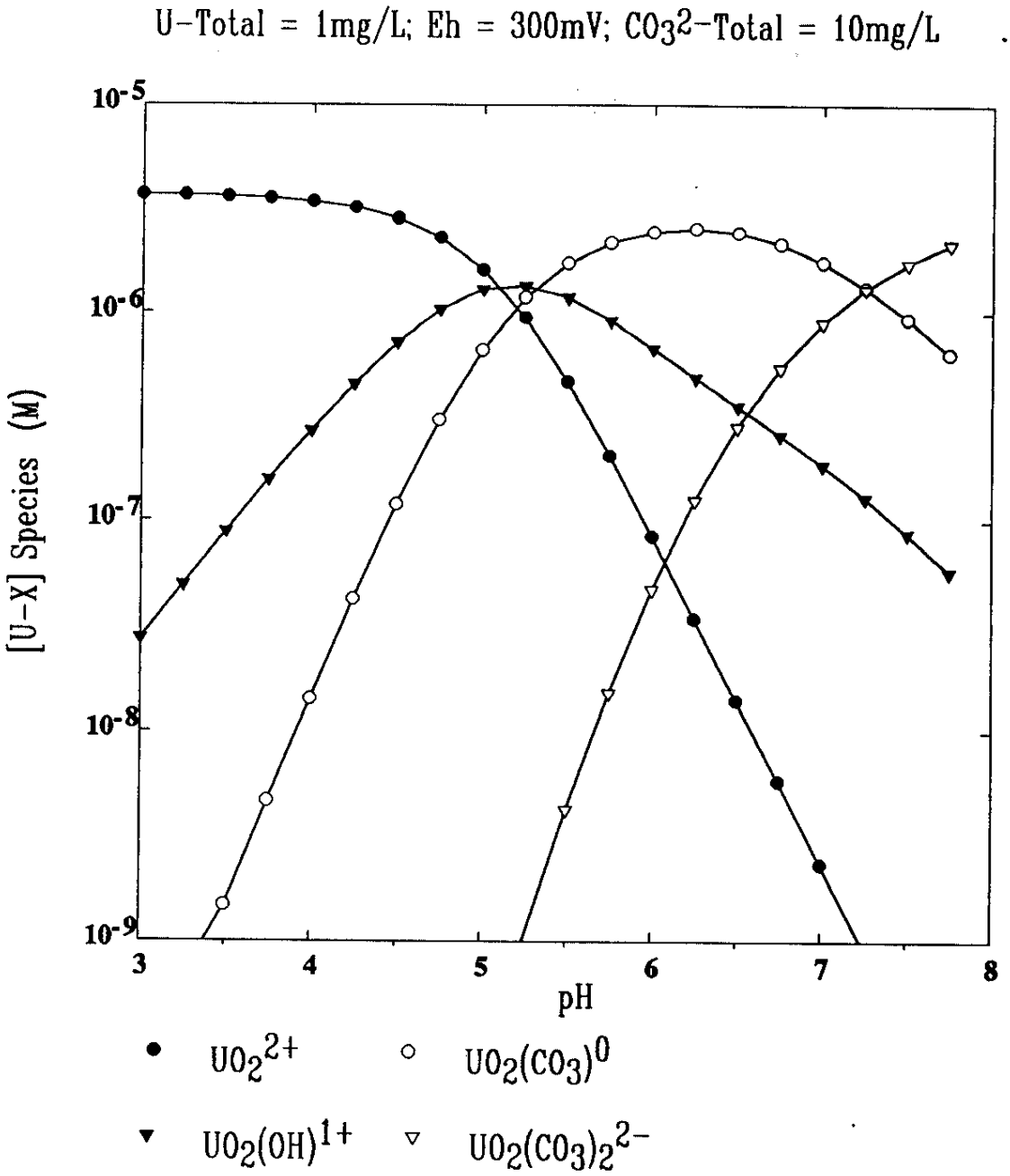

Figure 4-12. Field-derived distribution coefficients versus pH.

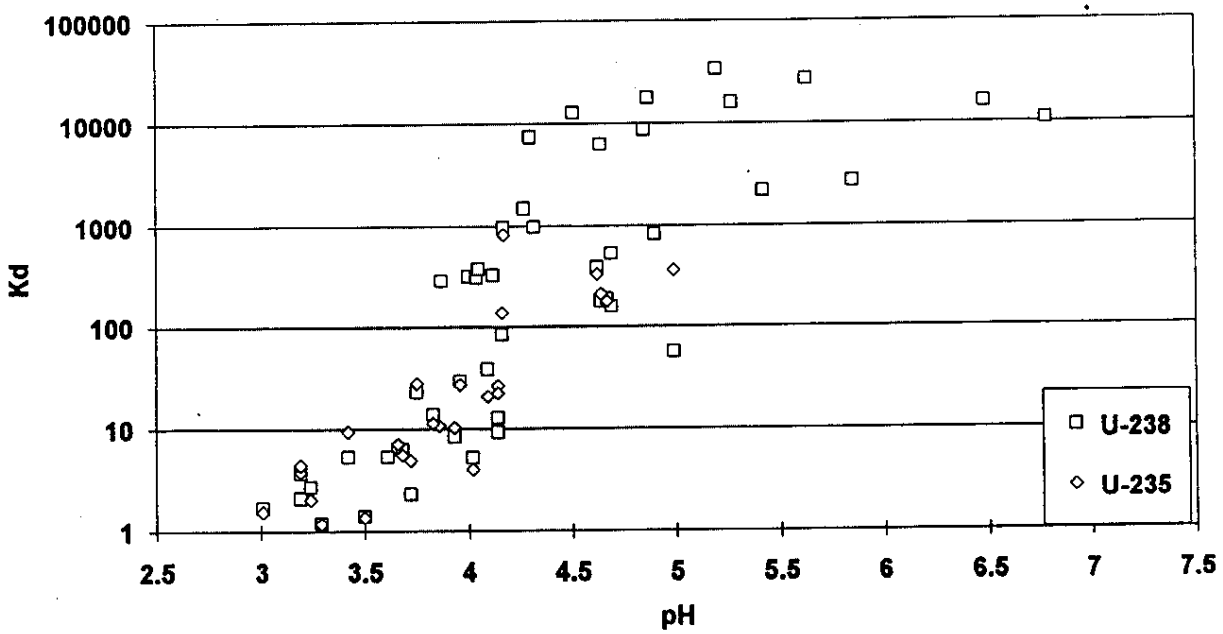

Figure 4-13. Field-derived uranium K_d values versus clay fraction in the soil.

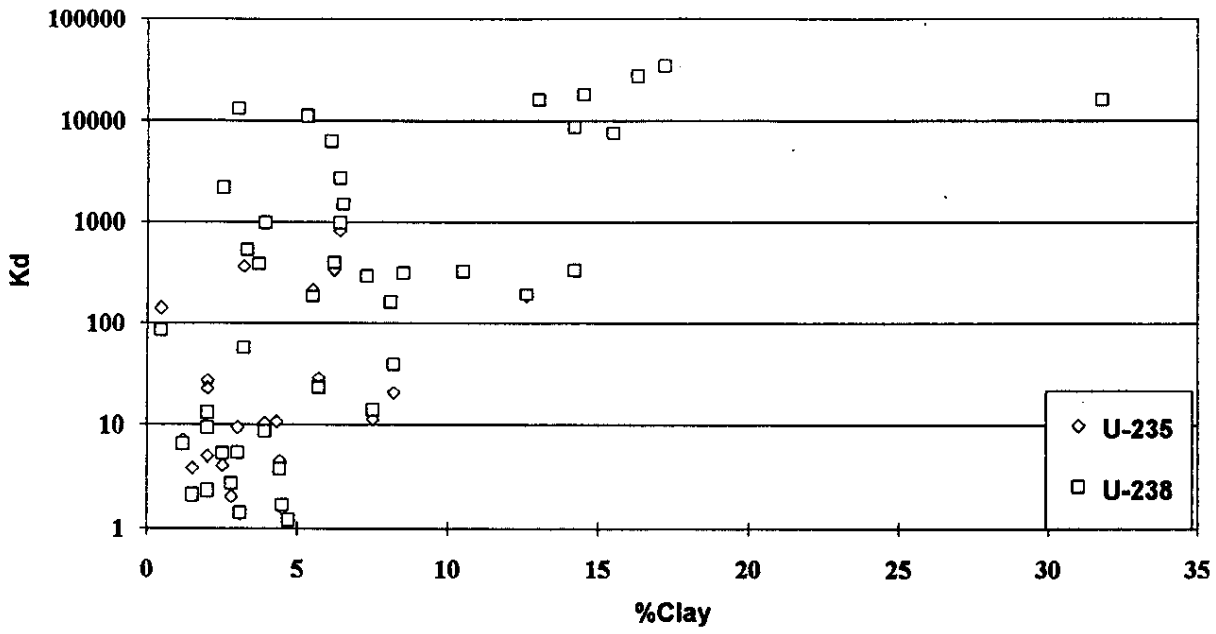

Figure 4-14. Field-derived uranium K_d values versus soil cation exchange capacity.

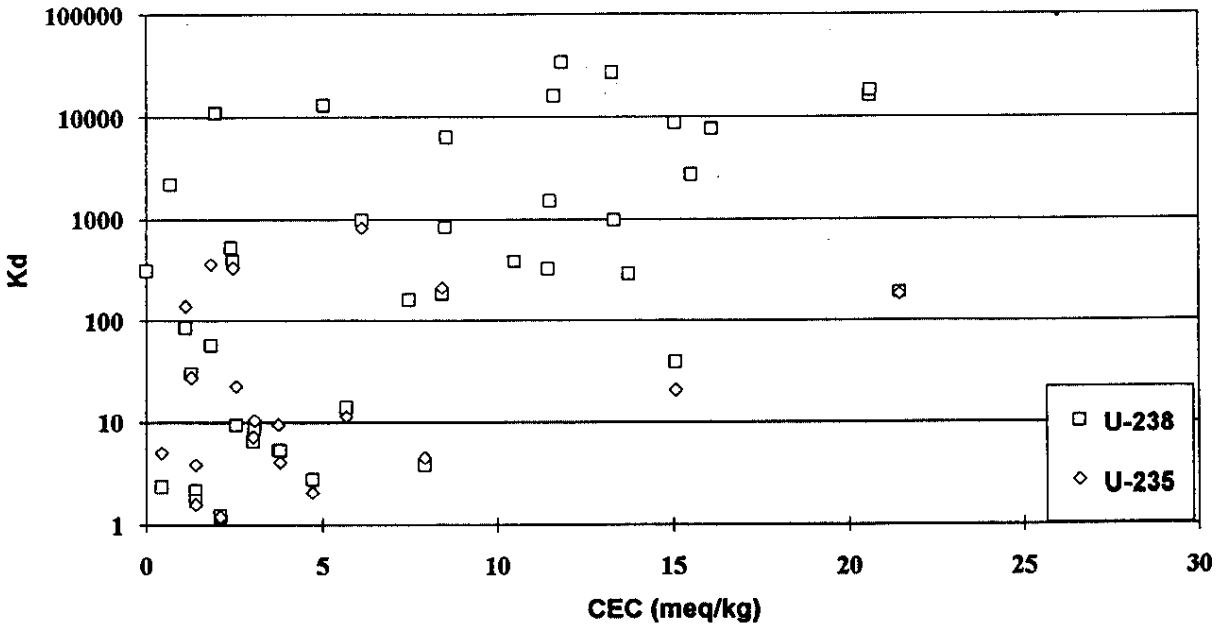

Figure 4-15. Linear uranium partitioning model of observed ^{238}U field data The curve shown below for $K_d = 3$ is the "best fit" concentration of sorbed uranium as predicted by the single K_d, one- and two-site Langmuir and constant capacitance models. The curve for $K_d = 40$ is the currently predicted uranium concentration.

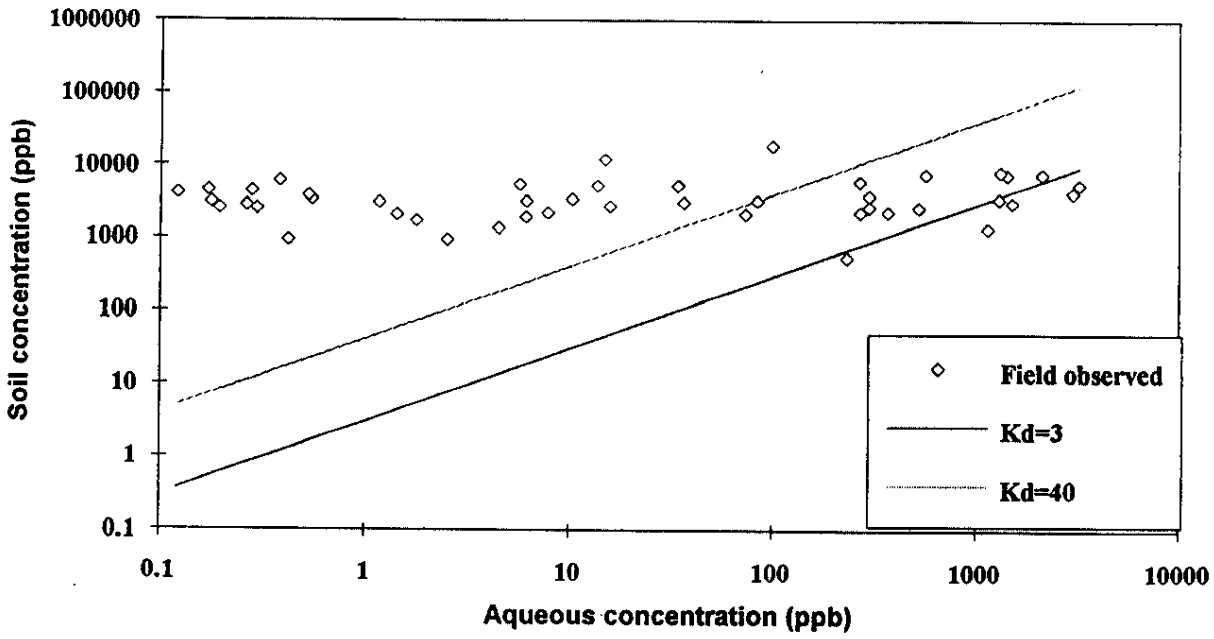

Figure 4-16. Variable-charge constant capacitance model of observed ^{238}U field data

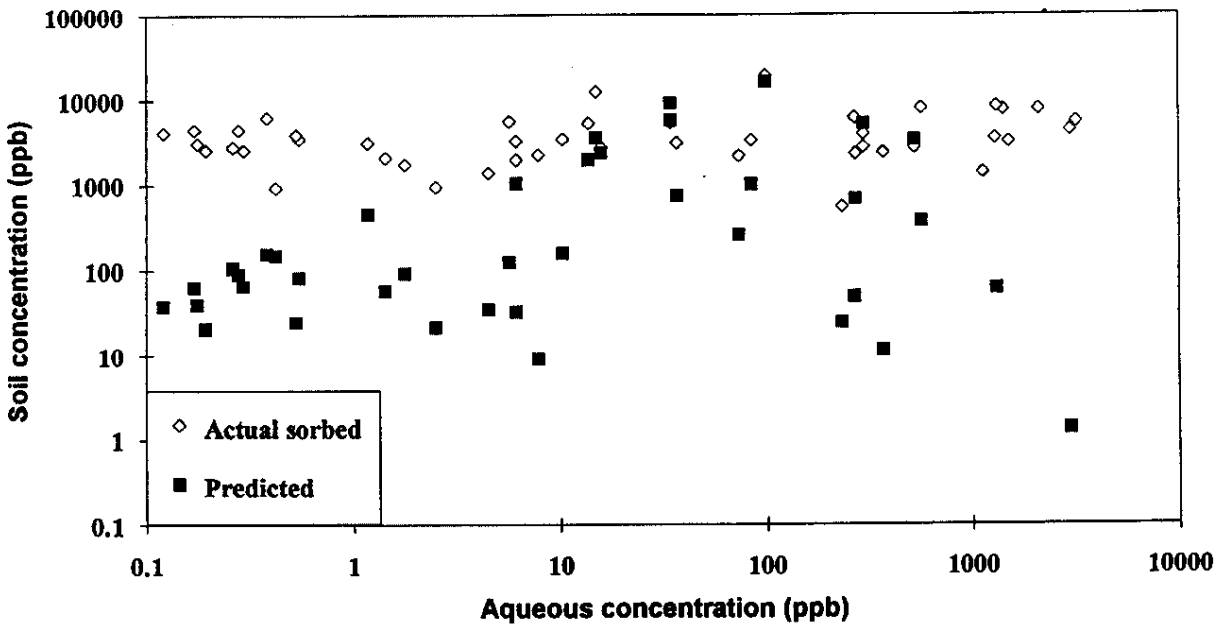

Figure 4-17. Diffuse-Layer model of observed ^{238}U field data

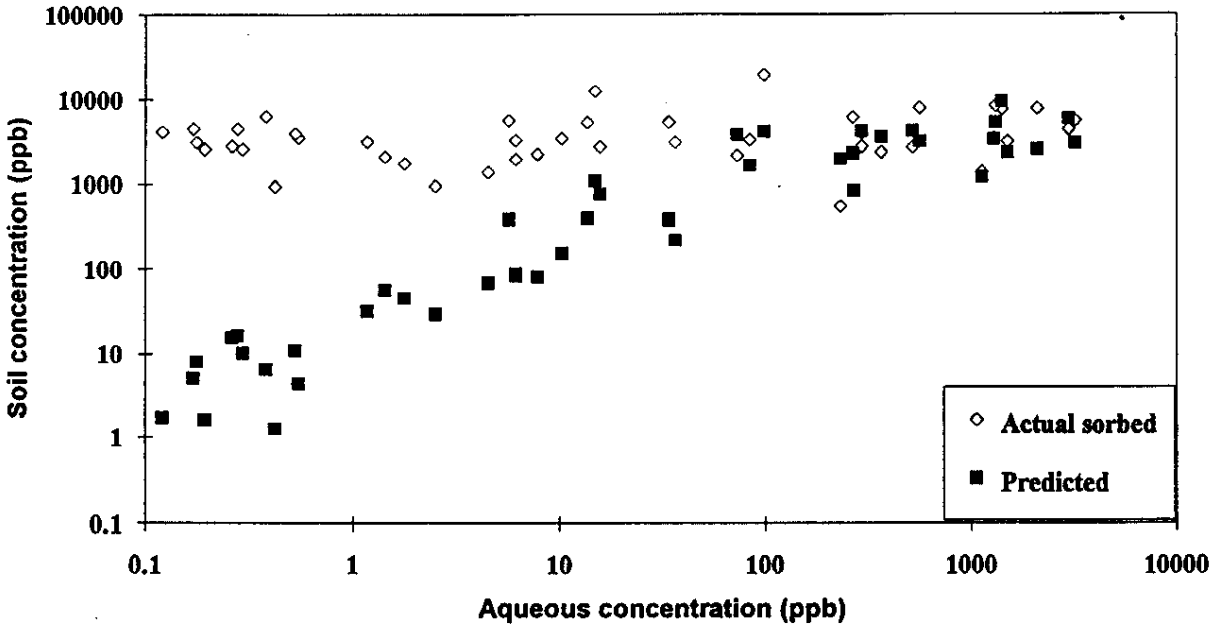

Figure 4-18. Variable-charge diffuse-layer model of ^{238}U observed field data

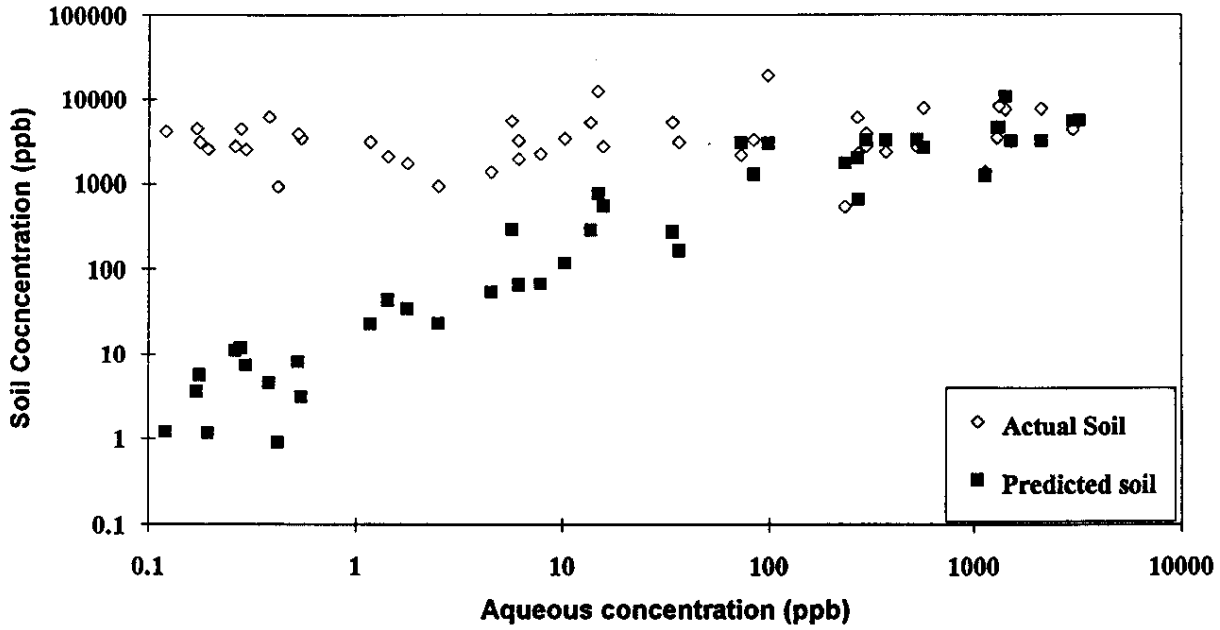

Figure 4-19. Empirical fitting of uranium sorption data.

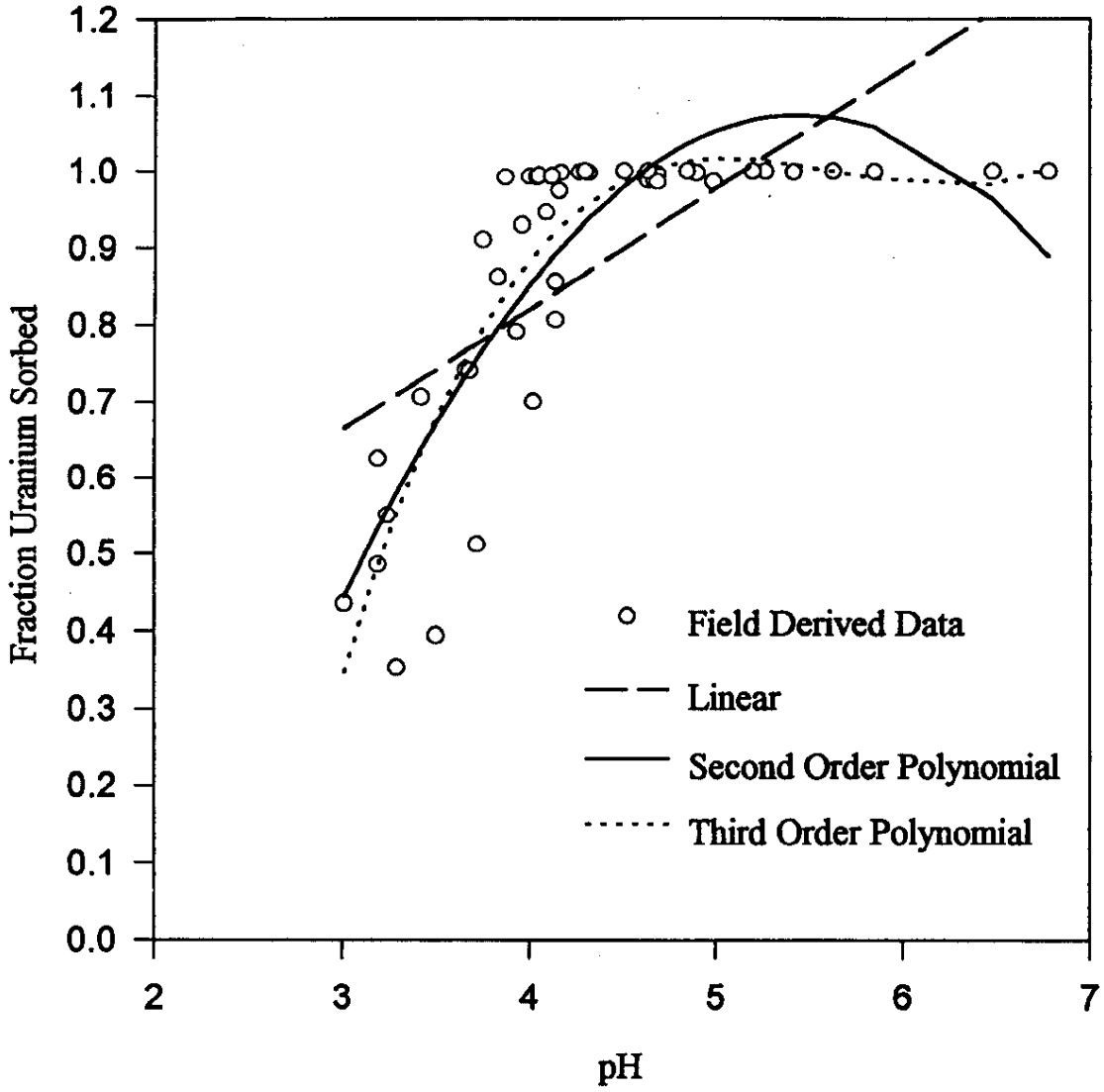

Figure 4-20. Isotherm for sorption of uranium on gibbsite as a function of pH.

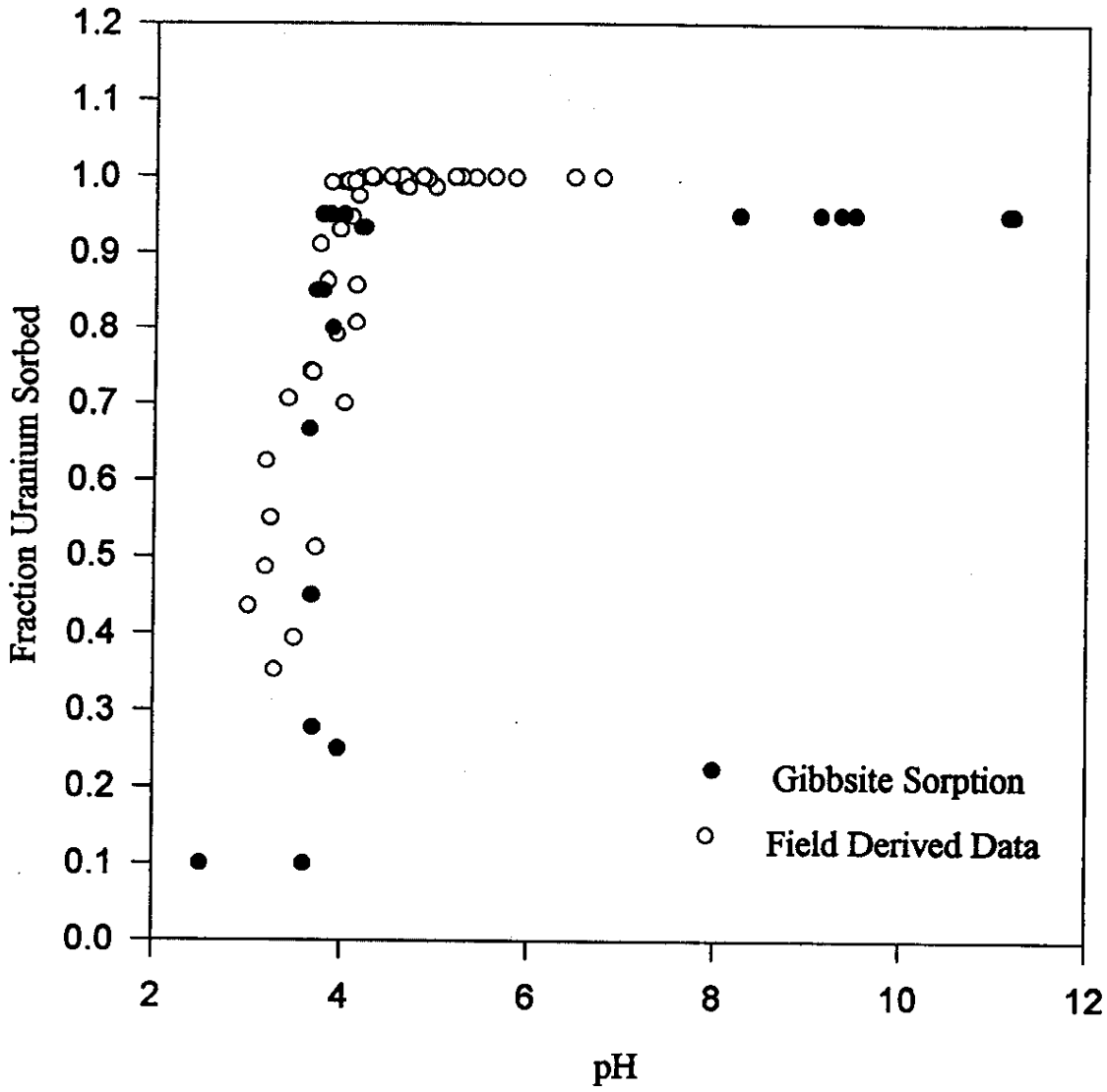

5.0 CONCLUSIONS

The partitioning of a contaminant between the aqueous and solid phases in natural systems can not be accurately described by a single linear isotherm. A simple method of obtaining site-specific distribution behavior of contaminants in a polluted aquifer is to analyze matched sets of porewater and soil samples. The site-specific distribution coefficients for the FHSB system determined using this method vary by several orders of magnitude. The soil concetrations (i.e. soil source term) are much smaller than earlier estimates used in modeling efforts.

In this study, uranium sorption is explained largely in terms of aqueous sample pH. In addition, the sorption isotherm for uranium shows a significant increase in sorption above pH 4.0, with K_d values range from about 1 to 34,000 at the FHSB.

The partitioning behavior of uranium to FHSB soils can not be explained in terms of the physical properties of the soils (i.e., particle size distribution, or cation exchange capacity). This suggests that surface mineral coatings are controlling uranium sorption at the seepage basins. Literature and experimental laboratory data of uranyl sorption to gibbsite and kaolinite are very similar to the field-derived data. Because sorption is not well correlated with the soil clay content or CEC, gibbsite, rather than kaolinite, is more likely the reactive mineral surface present at FHSB.

Aqueous-phase speciation modeling predicts that uranium should be present as uranyl ion (UO_2^{2+}) at low pH values and as $UO_2(OH)^+$ at pH values greater than about 5.0 in systems where carbonate is absent. For systems containing significant amounts of carbonate, uranyl cabonate ($UO_2CO_3^0$) becomes the dominant species above a pH value of 5.5. During remediation, it is anticipated that carbonate levels in the treated water will increase due to increasing pH values and exposure to the atmosphere.

Isotopic ratios of uranium indicate that the majority of uranium present is <u>not</u> naturally occurring. Uranium is depleted in F-Area and enriched in the soils in H-Area.

Finally, sorption isotherms generated from this study should be used to update risk analysis and estimates of remediation times. To more easily apply these data, stability constants for a variety of sorption models and empirical curves were fitted to the field-derived data. Empirical fitting of pH versus the fraction of uranium sorbed to a third order polynomial produced the best fit to the data. Of the mechanistic models applied, the diffuse-layer model provided the best fit to the data. The fit of data by this model, as measured by normalized error squared, was two orders of magnitude better than a single K_d of 40. Using the stability constant derived for the diffuse layer model ($K_{dlm} = 3.2$) and the aqueous uranium concentrations, the concentration of sorbed uranium can be calculated using eqn. 3-10.

6.0 IMPLICATIONS FOR REMEDIATION AND RECOMMENDATIONS

6.1 Further Work

6.1.1 *Soil Aging*

An experimental study has been initiated to examine the influence of modifying soil on the binding of heavy metals and radionuclides because processes like coprecitation and precipitation of fresh mineral phases are expected to influence binding of contaminants

For this work, approximately 8 kg of an uncontaminated soil collected upgradient of the FHSB, was packed into a column. Then, approximately 39 pore volumes (equivalent to 100 l) of deionized water was passed through the column at an average flow of about 6 pore volumes per day. The influent and effluent from the column was sampled to determine the concentrations of those elements which are easily leached.

Currently, a simulated FHSB waste solution is being passed through the column to allow the background soil to undergo a weathering process similar to that which is expected to occur for the FHSB soils. The simulated waste solution has a pH of 2.5 with 1000 ppm NO_3^- and about 300 ppm Na^+. Periodically, a small sample of the soil will be removed and batch studies on uranium, cadmium and cesium sorption will be conducted. This experiment will allow a comparison of the sorption behavior of modified soil as a function of waste solution volume. The results of this study will be used to help determine the extend of changes in the sorption behavior of an aquifer soil, for a given set of geochemical conditions, as an acidic plume moves through the aquifer.

6.1.2 *Sequential Extraction*

Knowledge of the types of soil binding sites to which uranium sorbs can lead to a more accurate prediction of uranium transport. In a future study, the sorption of uranium onto eight operationally defined "classes" of binding sites will be examined. In this study, a small portion of each soil sample will be sequentially leached using increasingly aggressive extractants. The contaminants removed with each extractant, will be classified as being bond to a particular, operationally defined, binding site. The 8 extractants and associated classes of sites are as follows:

1) water soluble constituents which can be removed by vigorous shaking in deionized water for 16 hours;
2) easily exchangeable constituents removed by vigorous shaking for 16 hours in 0.5 M $Ca(NO_3)_2$ solution;
3) specifically sorbed constituents which can be removed from the soil surfaces by a solution of 0.44 M CH_3COOH and 0.1 $Ca(NO_3)_2$ (8 hours);
4) contaminants associated with easily reducible metals such as ferrous iron and manganese oxides which can be removed with a solution of 0.01 M NH_2OH-HCl and 0.1 M HNO_3 (30 minutes);

5) organically bound contaminants which can be extracted with 0.1 M $Na_4P_2O_7$ (24 hours).
6) contaminants sorbed on the poorly crystalline aluminosilicates and hydrous oxides which can be extracted using a 0.175 M $(NH_4)_2C_2O_2$/0.1 M $C_2H_2O_4$ solution in the dark (4 hours);
7) contaminants associated with crystalline iron oxides which can be removed by reducing Fe^{3+} to Fe^{2+} with 0.75 g $Na_2S_2O_4$ and while complexing the ferrous iron in a citrate buffer made with 0.15 M $Na_3C_6H_5O_7$ and 0.05 M $HOC(CH_2CO_2H)_2CO_2H$ (30 minutes); and
8) residual constituents which are removed by a digestion in hot hydrofluoric acid and aqua regia.

The extractants from each step of the sequential extraction procedure will be analyzed using inductively coupled plasma-mass spectrometry (ICP-MS) to determine the concentrations of desired isotopes. A mass balance check of the sequential extraction procedure may be performed by comparing the concentration determined by the total digestion to the sum of the concentrations extracted in all of the sequential extraction steps.

The distribution coefficients reported in this work tend to overestimate uranium sorption because the uranium concentrations reported in the soil included not only the exchangeable uranium sorbed on the soil surface, but also that associated with the soil matrix. The sequential extraction procedure described above will allow better estimates of the true uranium partitioning. By assuming that only the uranium released with the final extraction is associated with the soil matrix, an more representative K_d value can be determined.

Future work could include extension of these data to other waste sites by indexing the type and quantity of soil sorption sites available. The development of operationally defined classes of binding sites, like those being used in the above described sequential extraction experiments, can provide a method for the accomplishment of this task.

6.2 Implications for Remediation

The most important implication of this work for the remediation of groundwater in the vicinity of the FHSB is that a pump and treat system can be predicted to work even more effectively than previously thought. This is due to the fact that the soil source term is much smaller than has been used in previous modeling efforts (GeoTrans 1991b). All other geochemical conditions being equal, this should result in a much shorter remediation time and a greater effectiveness of a pump-and-treat design than previously predicted.

A second implication of this work is that a remediation effort which is conducted in the near future could be more effective than one conducted later on. This is due to a gradual change in the groundwater chemistry due to the discontinuation of seepage basin operation. The inflection point of the uranium sorption isotherm occurs at about pH = 4.0

(i.e., at a pH below 4, most of the uranium is in solution, while above 4, most uranium is sorbed). Since a large fraction of the uranium at the site is associated with the low-pH portion of the plume, substantial portions of the total uranium mass could be more easily removed before the pH of the system returns to more natural conditions. Therefore, consideration could be given to pumping water from the lowest pH portions of the plume in the F-Area.

Finally, because uranium mobility is highly dependent on aqueous pH and carbonate concentration, a strategy that uses the chemistry of the reinjection water to either mobilize or immobilize contaminants could be developed. For this strategy, it would be essential to account for the buffering capacity of the soils when determining the rate of pH increase during remediation, and the effect of introducing more carbonate rich and higher pH waters into the injection zone on the uranium speciation and subsequent transport.

Acknowledgments: This research was supported by the U. S. Department of Energy under contact DE-AC09-89SR18035, administered by Westinghouse Savannah River Company, and under contract DE-AC09-76SR00819, administered by the University of Georgia's Savannah River Ecology Laboratory. William H. Johnson was supported by an appointment to the Nuclear Engineering and Health Physics Fellowship program administered by Oak Ridge Institute for Science and Education for the U. S. Department of Energy. Special thanks are extended all the individuals will assisted on this project. Ms. Lynn M. Johnson investigated uranium sorption onto gibbsite. Mr. Neil A. Johnson assisted with particle size analysis of soil samples and performed the x-ray diffraction work. Thank yous are extended to Ms. Aimee T. Buchanan and Ms. Mira Malek for assistance sample preparation and sorption studies. Ms. Amy L. Bryce performed surface area analysis and freeze drying of clay and idealized surface samples. Mr. Steve M. Mead and Mr. Mike D. McHood are to be thanked for their efforts in initiating sample collection.

7.0 REFERENCES

Allison, J. D., D. S. Brown and K. J. Gradac. 1991. MINTEQA2/PRODEFA2: A geochemical Assessment Model for Environmental Systems: Version 3.0 Users Manual. EPA/600/3-91/021. Washington, DC: U. S. Government Printing Office.

Anderson, P. R. and M. M. Benjamin. 1990. Surface and bulk characteristics of binary oxide suspensions. Env. Sci. Tech. 24:692-698.

ASTM. 1989. Standard test method for pH of soils. American Society for Testing and Materials. ASTM-D4972-89.

Bear, F. E. 1964. Chemistry of the soil. New York: Reinhold Publishing.

Corbo, P., M. V. Kantelo, and C. B. Fliermans. 1985. Analytical results, database managment and quality assurance for analysis of soil cores from the F- and H-Area Seepage Basins. DPST-85-921. E. I. DuPont de Nemours & Company; Aiken, SC.

Davis, J. A., R. O. Davis, and J. O. Leckie. 1978. Surface Ionization and Complexation at the Oxide/Water Interface I. Computation of Electric Double Layer Properties in Simple Electrolytes. J. Colloid Interface Sci. 63:480-499.

Edge, R. W. and K. Cordy. 1989. The Hydropunch: An In Situ Sampling Tool for Collecting Ground Water From Unconsolidated Sediments. Groundwater Monitoring Reviews 9:177-183.

Gee, G. W. and J. W. Bauder. 1986. Particle size analysis. In: Klute, A. ed. Methods of soil analysis, part 1. Physical and mineralogical methods. Madison, WI: Soil Science Society of America, pp. 383-412.

GeoTrans, Inc. 1991a. Baseline CERCLA risk assessment: F & H Area Seepage Basins Groundwater Unit. WSRC-RP-91-1017.

GeoTrans, Inc. 1991b. Groundwater Monitoring of Remedial Alternatives for the F- and H-Area Seepage Basins. 3017-002. Geo Trans, Inc., Sterling, VA.

Hayes, K. F., G. Redden, W. Ela, and J. O. Leckie. 1990. Application of surface complexation models for radionuclide adsorption. NUREG\CR-5547.

Inoue, Y. and W. J. Kaufman. 1963. Prediction of Movement of Radionuclides in Solution Through Porous Media. Health Physics 9:705-715.

Johnson, N. A. 1994. Clay mineralogy of the surficial aquifer and confining system, F- and H-Area Seepage Basins, Savannah River Site. Gainesville, FL: Dept. of Geology, University of Florida.

Langmuir, D. 1979. Uranium Solution-Mineral Equilibria at Low-Temperatures with Application to Sedimentary Ore Deposits. Geochim. Cosmochim. Acta 42:547-569.

Lim, C. H. and M. L. Jackson. 1982. Dissolution for total elemental analysis. In: Page, A. L., R. H. Miller and D. R. Jackson, eds. Methods of soil analysis, part 2. Chemical and mircobiological properties. Madison, WI: Soil Science Society of America, pp. 1-11.

Looney, B. B., Grant M. W., King, C. M. 1985. Estimation of geochemical parameters for assessing subsurface transport at the Savannah River Plant. DSPT-85-904. E. I. du Pont de Nemours & Co., Aiken, SC.

Reardon, E. J. 1981. K_d's - Can They Be Used to Describe Reversible Ion Sorption Reactions in Contaminant Migration? Groundwater 19:279-286.

Rhoades, J. D. 1982. Cation exchange capacity. In: Page, A. L., R. H. Miller and D. R. Jackson, eds. Methods of soil analysis, part 2. Chemical and mircobiological properties. Madison, WI: Soil Science Society of America, pp. 149-157.

Ryan, J. P. 1984. Effluent characterization study for the 200-Area Effluent Treatment Facility. DPST-84-511. E. I. DuPont de Nemours & Company; Aiken, SC.

Soil Survey Staff. 1975. Soil taxonomy: A basic system of soil classification for marking and interpreting soil surveys. USDA-SCS Agric. Handbook 436. Washington, DC: U. S. Government Printing Office.

Stumm, W. and J. J. Morgan. 1981. Aquatic chemistry. New York: John Wiley & Sons.

Stumm, W. 1992. Chemistry of the solid-water interface. New York: John Wiley & Sons.

Van Genuchten, M. T, J. M. Davidson, and P. J. Wierenga. 1974. An evaluation of kinetic and equilibrium equations for the prediction of pesticide movement through porous media. Soil Sci. Soc. Amer. J. 38:29-35.

WSRC. 1992a. Redmedial Action Alternative Risk Assessment for the F- and H-Area Seepage Basins Groundwater Unit. Vol II. Appendices A-I: Exposure assessment data. WRSC-RP-91-1017. Westinghouse Savannah River Company, Aiken, SC.

WSRC. 1992b. F-Area Seepage Basins Groundwater Monitoring Report: Third quarter 1992. WRSC-TR-92-509. Westinghouse Savannah River Company, Aiken, SC.

WSRC. 1992c. H-Area Seepage Basins Groundwater Monitoring Report: Third quarter 1992. WRSC-TR-92-510. Westinghouse Savannah River Company, Aiken, SC.